공학박사 학위논문

Effective Realization of Time-Dependent Monte Carlo Simulation Method for Nuclear Reactor Transient Analysis

원자로 과도상태 해석을 위한 효과적인 시간종속

몬테카를로 중성자 모의법 개발

2017 년 8 월

서울대학교 대학원

에너지시스템 공학부

Nadeem Shaukat

Effective Realization of Time-Dependent Monte Carlo Simulation Method for Nuclear Reactor Transient Analysis

지도 교수 심 형 진

이 논문을 공학박사 학위논문으로 제출함

2017 년 8 월

서울대학교 대학원

에너지시스템 공학부

쇼컷 나딤

Nadeem Shaukat 의 공학박사 학위논문을 인준함

2017 년 8 월

위 원 장 주한규 (인)

부위원장 심형진 (인)

위 원 조형규 (인)

위 원 이덕중 (인)

위 원 박창제 (인)

Abstract

Effective Realization of Time-Dependent Monte Carlo Simulation Method for Nuclear Reactor Transient Analysis

Nadeem Shaukat

Nuclear Engineering Ph.D.

Energy Systems Engineering

Seoul National University

The asymptotic time behavior of neutron transport can be assessed by studying the several issues regarding the reactor start-up analysis, reactivity measurements or the kinetic study of accelerator-driven systems. This amounts to solve the time-dependent Boltzmann neutron transport equation. The time-dependent Monte Carlo (TDMC) algorithm with conventional combing method is implemented in the McCARD.

The α-eigenvalue is estimated from the TDMC calculations for subcritical systems. The effectiveness of the results is examined for the rod model and two-group infinite homogeneous problems with varying the k-value by comparisons with analytical solutions. The applicability of the TDMC

module is also evaluated for an experimental benchmark of the thorium-loaded accelerator-driven system at Kyoto University Critical Assembly (KUCA) by comparisons of α's calculated by the DMC simulations with those from the measurements, the MC α iteration algorithm and the MC PNS simulations.

With ever-advancing computer technology, the Monte Carlo (MC) neutron transport calculation is expanding its application area to the nuclear reactor transient analysis. The TDMC neutron tracking for the transient analysis requires efficient algorithms for delayed neutron generation, neutron population control, and modeling of initial conditions. In this study, a new MC steady-state simulation method based on the time-dependent MC (TDMC) neutron tracking is proposed for the steady-state initial condition modeling from which prompt neutron sources and delayed neutron precursors for the MC transient simulation can be easily sampled. For the transient analysis, the proposed TDMC steady-state simulation method has been implemented in McCARD and applied for two-dimensional core kinetics problems in the time-dependent neutron transport benchmark, C5G7-TD without temperature feedback. The McCARD TDMC calculation results show good agreements with results of a deterministic transport analysis code, nTRACER. The reactor core transient analysis also requires neutronics calculations with the thermal-hydraulic (TH) feedback. In this study, the McCARD code with TDMC

scheme for the core transient analysis has been implemented by coupling with a computational fluid dynamics code, CUPID using the TCP/IP socket communication. In the McCARD/CUPID transient calculations, temperature-dependent cross sections are produced by a built-in on-the-fly Doppler broadening (OTF DB) module. The effectiveness of McCARD/CUPID transient analysis results is examined for a hypothetical triangular unit cell problem in the IAEA coordinated research project (CRP) benchmark on the high temperature gas cooled reactor (HTGR) uncertainty analysis.

The statistical uncertainty of one time step is estimated with the uncertainty propagating through the calculation from the preceding time step. With the help of formal uncertainty propagation approach, it is investigated that how the uncertainty occurs in the desired quantity of the system.

Keywords:

Time-Dependent Monte Carlo (TDMC)

Alpha Eigenvalue Estimation

Transient Analysis of Nuclear Reactor

C5G7-TD Benchmark

Uncertainty Propagation

Student Number: 2013-30779

Contents

Abstract i
Contents vi
List of Figures viii
List of Tables xi
CHAPTER. 1 Introduction 1
1.1 Background 1
1.2 Objective and Structure of the Thesis 4
CHAPTER. 2 Alpha Eigenvalue Estimation from Time-Dependent Monte Carlo Calculation for Off-Critical Systems 7
2.1 Neutron History-Based Time-Dependent Monte Carlo Scheme 7
2.2 Mathematical Formulation of Neutron Density Tally 9
2.2.1 Definition of Scale Factor 10
2.2.2 Recursive Formulation of Scale Factor 11
2.3 Estimation of Prompt Neutron Decay Constant Alpha 13
2.4 Numerical Results 16
2.4.1 The Rod Model 16
2.4.2 Numerical Results for Infinite Homogeneous Two-Group Problems 18
2.4.3 Application to Th-ADS Experimental Benchmarks 22
CHAPTER. 3 The Time-Dependent Monte Carlo Algorithm for the Transient Analysis of Nuclear Reactors 28
3.1 Coupled System of Equations for Transient Analysis of Nuclear Reactor 28
3.2 TDMC Steady-State Simulation 30

3.3 Numerical Results for the Transient Analysis without Temperature Feedback for the OECD/NEA C5G7-TD Benchmark 35
3.3.1 C5G7-TD Application Results 35
3.3.2 TDMC Steady-State Calculation 38
3.3.3 2-D Transient Problems 42
3.3.3.1 C5G7 Exercise 0 (TD0) 42
3.3.3.2 C5G7 Exercises 1 and 2 (TD1 and TD2) 46
3.3.3.3 C5G7 Exercise 3 (TD3) 49
3.3.4 3-D Transient Problems 53
3.3.4.1 C5G7 Exercise 4 (TD4) 53
3.3.4.2 C5G7 Exercise 5 (TD5) 59
3.4 Numerical Results for the Transient Analysis with Temperature Feedback for the IAEA CRP HTGR UAM Benchmark 64
3.4.1 IAEA CRP HTGR UAM Benchmark (Triangular Unit Cell Model) 65
3.4.2 Numerical Results 67
CHAPTER. 4 Uncertainty Propagation Analysis for the Dynamic Monte Carlo Simulations 70
4.1 Uncertainty Propagation in Neutron Density Tally 70
4.2 Numerical Results 73
4.2.1 The Rod Model 73
4.2.2 Infinite Homogeneous Two-Group Problem 79
CHAPTER. 5 Conclusions and Future Work 86
5.1 General Conclusions 86
5.2 Validation 88
5.3 Further Developments 89
References 91

List of Figures

Figure 2.1: Division of history based neutron simulation in time 8
Figure 2.2: Time-dependent neutron density tally 12
Figure 2.3: Neutron transport through one dimensional infinite homogeneous media 17
Figure 2.4: Convergence of alpha using TDMC simulations for different k_p values 21
Figure 2.5: Core configurations with 14 MeV pulsed neutrons for Th-ADS experimental benchmarks. (a). Th-PE, Th-Gr, Th-Be, Th-HEU-PE, and NU-PE 24
Figure 2.6: TDMC neutron flux for the Th-ADS benchmark problems 25
Figure 2.7: Convergence of alpha using TDMC simulations for the Th-ADS benchmark problems 26
Figure 3.1: Flow chart of the TDMC steady-state calculation at time step i 34
Figure 3.2: 2D core configuration for the C5G7-TD benchmark 37
Figure 3.3: k_{eff} convergence plots of the TDMC steady-state calculations for 2D C5G7-TD with varying the time step intervals as 0.0001, 0.001, 0.01, 0.05, 0.1, 1.0 and 2.5 ms 40
Figure 3.4: Comparison of converged k_{eff} values calculated by the TDMC steady-state simulations for 2D C5G7-TD according to the time step interval 40
Figure 3.5: Comparison of flux spectra with varying the time step interval in the TDMC steady-state simulations for the 2D C5G7-TD core 41

Figure 3.6: Comparisons of dynamic reactivities calculated by McCARD and nTRACER for problems TD0-1 and TD0-5 44
Figure 3.7: Comparisons of fractional total fission rates calculated by McCARD and nTRACER for problems TD0-1 and TD0-5 45
Figure 3.8: Comparisons of dynamic reactivities calculated by McCARD and nTRACER for problems TD1-1 and TD2-1 47
Figure 3.9: Comparisons of fractional total fission rates calculated by McCARD and nTRACER for problems TD1-1 and TD2-1 48
Figure 3.10: Core moderator density changes in the TD3 problems 50
Figure 3.11: Comparisons of dynamic reactivities calculated by McCARD and nTRACER for the TD3 problems 51
Figure 3.12: Comparisons of fractional total fission rates calculated by McCARD and nTRACER for the TD3 problems 52
Figure 3.13: Relative depth of control bank movement in TD4-1 and TD4-5 problems 54
Figure 3.14: Comparisons of dynamic reactivities calculated by McCARD and nTRACER for TD4-1 problem 55
Figure 3.15: Comparisons of dynamic reactivities calculated by McCARD and nTRACER for TD4-5 problem 56
Figure 3.16: Comparisons of fractional total fission rates calculated by McCARD and nTRACER for TD4-1 problem 57
Figure 3.17: Comparisons of fractional total fission rates calculated by McCARD and nTRACER for TD4-5 problem 58
Figure 3.18 Relative moderator density changes in the TD5 problems 61
Figure 3.19: Comparisons of dynamic reactivities calculated by McCARD and nTRACER for the TD5 problems 62

Figure 3.20: Comparisons of fractional total fission rates calculated by McCARD and nTRACER for the TD5 problems 63
Figure 3.21: Thermal-hydraulics coupling scheme of McCARD/CUPID 65
Figure 3.22: Triangular unit cell model 66
Figure 3.23: Temperature profile at the initial condition 68
Figure 3.24: Power density and temperature profile 69
Figure 4.1: Exponential variation of neutron density tally with time 77
Figure 4.2: Standard deviation vs real standard deviation 77
Figure 4.3: Neutron density in first energy group 82
Figure 4.4: Neutron density in second energy group 82
Figure 4.5: Standard deviation vs real standard deviation. 83

List of Tables

Table 2.1: One group cross-sections for infinite homogeneous super critical system 17
Table 2.2: Comparisons of α estimates for the one-group infinite homogeneous problem 17
Table 2.3: Cross sections for the two-group infinite homogeneous problem [3] 19
Table 2.4: Prompt criticality k_p with the varying differential scattering cross section of the first group [3] 19
Table 2.5: Comparisons of α estimates for the two-group infinite homogeneous problem 20
Table 2.6: k_{eff}*'s* of the seven core configurations 23
Table 2.7: Comparison of the α eigenvalues for the Th-ADS experimental benchmarks 27
Table 3.1: Number densities of nuclides 67
Table 4.1: One-group cross sections for infinite homogeneous problem 74
Table 4.2: Comparison of neutron densities for one-group infinite homogeneous problem 76
Table 4.3: Comparison of Standard Deviation and Real Standard Deviation in Neutron Densities 78
Table 4.4: Two-group cross sections for infinite homogeneous problem 81
Table 4.5: Comparison of neutron densities for two-group infinite homogeneous problem 84
Table 4.6: Comparison of standard deviation and real standard deviation in neutron densities 85

CHAPTER. 1 Introduction

1.1 Background

The transient analysis of a nuclear reactor is one of the ultimate goals of Monte Carlo (MC) neutron transport calculations. Recently, the MC transient analyses have been conducted by two kinds of approaches – the Dynamic MC (DMC) method with simulating delayed neutron precursors [1,2] and the quasi-static method in which MC neutron transport calculations are used to estimate the angular neutron flux at a fixed time [3]. The quasi-static method is afforded to efficiently solve a transient problem but may suffer from the time-discretization approximation. The time-dependent MC (TDMC) methods can handle the time variable of the neutron density or flux in its continuous domain by updating event times during the MC tracking of neutrons.

Since Kaplan [4] proposed an efficient matrix method utilizing the TDMC neutron tracking to estimate the time constant or α-eigenvalue of a nuclear system in 1958, reactor analysis applications of the TDMC methods have been limited to MC simulations of research reactors including critical assemblies to obtain kinetic physics parameters such as α-eigenvalue, kinetics parameters, noise data, etc. KENO-NR, a variant of KENO-V.a [5], and MCNP [6] were used [7-9] to generate time-dependent detector responses in

numerical simulations of noise experiments and the pulsed neutron source experiments. The TART code [10] is equipped with a TDMC algorithm in which the time domain is split into time bins and the neutron population in each time bin is controlled by the combing technique [11,12]. Cullen [12] compared the α-eigenvalues estimated by the TART's TDMC calculations with those by the α-static algorithm [13] for Godiva-like problems. For the experimental benchmarks on thorium-loaded accelerator-driven system [14], the present authors [15] compared the α-eigenvalues calculated by the TDMC method and the α iteration algorithm [16] using McCARD [17] with the experimental results. The Godiva super-prompt-critical burst experiment has been simulated by the Serpent-OpenFoam coupled system considering thermal feedback [18].

As noted by Sjenitzer and Hoogenboom [1], challenges of the MC reactor transient analysis include an effective generation of delayed neutrons, neutron population control, modeling of initial conditions, etc. Because the delayed neutron plays an important role in the transient behavior of reactor core characteristics in spite of its small generation fraction from a fission reaction, a special treatment for its time-dependent generation is required to reduce the statistical uncertainty expected to be high by a direct sampling of its delayed-generation time at each fission site. In order to overcome this

problem, Sjenitzer and Hoogenboom [1] developed a clever algorithm of MC tracking and forced decay of delayed neutron precursors. The second issue of the neutron population control have been approached by two ways in terms of a simulation of the branching process such as the fission reaction – an analog MC simulation in which extra neutrons from a fission are sampled and tracked accompanied with a time bin-wise population control technique such as the combing algorithm, and the branchless method [1] where the neutron weight is increased in accordance with the expected number of fission neutrons at each collision site. In this study, we apply the Sjenitzer and Hoogenboom's delayed neutron handling algorithm and the analog MC branching process simulation method with the combing technique [12] for the DMC transient analysis.

For the modeling of an initial condition of a transient scenario which is generally the steady-state condition, one may conduct the MC power iteration calculation [19] to obtain the fundamental-mode distribution of initial source neutrons and the fundamental-mode eigenvalue, k. In this work, we proposed a TDMC steady-state simulation method for the steady-state initial condition modeling as an alternative to the MC eigenvalue calculation.

The reactor core transient analysis also requires neutronics calculations with the thermal-hydraulic (TH) feedback. Sjenitzer and Hoogenboom have

already coupled the Monte Carlo code to a sub-channel code, which is a fast thermal-haydraulics code but not a high-fidelity code [2]. In this study, a TDMC scheme for the core transient analysis is coupled with a computational fluid dynamics code, CUPID [20] using the TCP/IP socket communication.

1.2 Objectives and Structure of the Thesis

The prompt neutron decay constant (referred to as α) is a directly-measurable parameter in reactor physics experiments such as the pulsed neutron method, the reactor noise method, and the exponential method. Calculation of the α by Monte Carlo method is usually performed by neutron transport calculations with a fixed neutron source. From the simulations of the pulsed neutron source (PNS) method or the exponential experimental method [21, 22], the α can be estimated. The α can alternatively be calculated by the α-k iteration algorithm [22] and α iteration algorithm [16], which has already been implemented in the Seoul National University MC code, Monte Carlo Code for Advanced Reactor Design and Analysis (McCARD) code [17].

In Chapter 2, conventional time-dependent Monte Carlo (TDMC) algorithm is implemented. There is an exponential growth of neutron population in estimation of neutron density tally for super-critical systems and the number of neutrons being tracked exceed the memory of the computer. In order to control this exponential growth at the end of each time boundary, a

conventional combing method for controlling population is included in TDMC [12]. A scale factor is introduced to tally the desired neutron density at the end of each time boundary. The main focus of this chapter is to estimate the α eigenvalue from the TDMC calculations for subcritical systems. The effectiveness of the results is examined for two-group infinite homogeneous problems with varying the *k*-value by comparisons with analytical solutions. The applicability of the TDMC module is also evaluated for an experimental benchmark of the thorium-loaded accelerator-driven system [14] at Kyoto University Critical Assembly (KUCA) by comparisons of α's calculated by the TDMC simulations with those from the measurements, the MC α iteration algorithm and the MC PNS simulations.

In Chapter 3, we apply the Sjenitzer and Hoogenboom's delayed neutron handling algorithm and the analog MC branching process simulation method with the combing technique [12] for the TDMC transient analysis. For the modeling of an initial condition of a transient scenario which is generally the steady-state condition, one may conduct the MC power iteration calculation [19] to obtain the fundamental-mode distribution of initial source neutrons and the fundamental-mode eigenvalue, *k*. The TDMC algorithms including the proposed steady-state simulation method have been implemented in McCARD [17] and applied for a time-dependent neutron transport benchmark

based on the well-known steady-state C5G7 benchmark problems, shortly the C5G7-TD benchmark [23]. The McCARD TDMC results for the C5G7-TD benchmark are compared with those from a deterministic transport analysis code, nTRACER [24]. A TDMC scheme for the core transient analysis including feedback has been implemented by coupling with a computational fluid dynamics code, CUPID [20] using the TCP/IP socket communication. In the McCARD/CUPID transient calculations, temperature-dependent cross sections are produced by a built-in on-the-fly Doppler broadening (OTF DB) module and applied to a triangular unit cell problem in the IAEA coordinated research project (CRP) benchmark on the high temperature gas cooled reactor (HTGR) uncertainty analysis [25].

In Chapter 4, we quantify the uncertainty propagation in neutron densities at the end of each time boundary for super-critical systems. This uncertainty is caused by the uncertainty resulting from the introduction of scale factor. The effectiveness of TDMC is examined for one-group infinite homogeneous problem (the rod model) and two-group infinite homogeneous problem.

Finally, Chapter 5 gives conclusions of the proposed methodologies and an outlook to possible further developments and improvements in the proposed methodologies to enhance the capability of the TDMC scheme.

CHAPTER. 2 Alpha Eigenvalue Estimation from Time-Dependent Monte Carlo Calculation for Off-Critical Systems

2.1 Neutron History-Based Time-Dependent Monte Carlo Scheme

In this study, the TDMC method is implemented, which is based on neutron history, thus it can also be called as neutron history based method (NHBM). In this method, all the neutron histories are tracked successively from the very beginning of time boundary to the end of each time boundary when all of its progenies are disappeared. In the TDMC simulations with the combing technique [12], each neutron is simulated time step-by-step with updating its time variable whenever its track is sampled by

$$t_p^{i,j} = t_{p-1}^{i,j} + \frac{l_p^{i,j}}{\sqrt{2E_p^{i,j}/m_n}} \tag{2.1}$$

where $t_{p'}^{i,j}$ ($p' = p$ or $p-1$), $l_p^{i,j}$, and $E_p^{i,j}$ are the time after the p'^{th} flight, the length and the neutron energy of the p^{th} track of history j at time step i. m_n is the neutron mass. If the sampled time is greater than or equal to the upper time bound of the i^{th} time step, i.e. $t_p^{i,j} > T_{i+1}$, then the track length of, and time after

the last flight P of history j, denoted by $l_P^{i,j}$ and $t_P^{i,j}$, respectively, become;

$$l_P^{i,j} = \left(T_{i+1} - t_{P-1}^{i,j}\right) \cdot \sqrt{2E_P^{i,j}/m_n} \tag{2.2}$$

$$t_P^{i,j} = T_{i+1} \tag{2.3}$$

where $E_P^{i,j}$ means the neutron energy of the last flight of history j at time step i. After the i^{th} time step TDMC simulations for all histories, the number of neutrons for the next time step simulations are controlled to be the user-provided number of histories by Russian roulette or splitting depending on the number of survived neutrons. Figure 2.1 shows an example of a simulated neutron history at time step i.

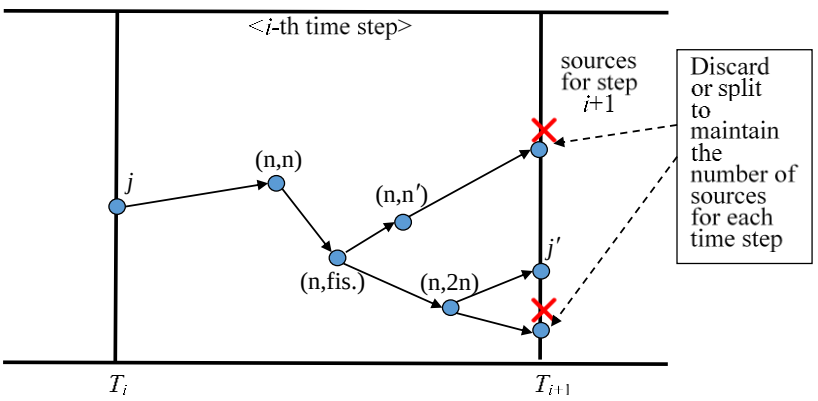

Figure 2.1: Division of history based neutron simulation in time

2.2 Mathematical Formulation of Neutron Density Tally

An integral form of the time-dependent Boltzmann transport equation for the collision density ψ(P), where **P** denotes the state vector of a neutron in the seven-dimensional phase space (three in space, two in direction, and one each in energy and time) $(\mathbf{r}, E, \hat{\mathbf{\Omega}}, t)$ can be written as;

$$\psi(\mathbf{P}) = \tilde{S}(\mathbf{P}) + \int d\mathbf{P}' K(\mathbf{P}' \to \mathbf{P}) \psi(\mathbf{P}') \tag{2.4a}$$

where

$$\psi(\mathbf{P}) = \Sigma_t(\bar{\mathbf{r}}, E)\, \phi(\bar{\mathbf{r}}, E, \hat{\mathbf{\Omega}}, t) \tag{2.4b}$$

$$K(\mathbf{P}' \to \mathbf{P}) = C(\bar{\mathbf{r}}', t'; E', \hat{\mathbf{\Omega}}' \to E, \hat{\mathbf{\Omega}})\, T(E, \hat{\mathbf{\Omega}}, t; \bar{\mathbf{r}}' \to \bar{\mathbf{r}}) \tag{2.4c}$$

$$C(\bar{\mathbf{r}}', t'; E', \hat{\mathbf{\Omega}}' \to E, \hat{\mathbf{\Omega}}) = \sum_r \frac{\Sigma_r(\mathbf{P}')}{\Sigma_t(\mathbf{P}')} \nu_r f_r(E', \hat{\mathbf{\Omega}}' \to E, \hat{\mathbf{\Omega}}) \tag{2.4d}$$

$$\begin{aligned} &T(E, \hat{\mathbf{\Omega}}, t; \bar{\mathbf{r}}' \to \bar{\mathbf{r}}) \\ &= \frac{\Sigma_t(\bar{\mathbf{r}}, E)}{|\bar{\mathbf{r}} - \bar{\mathbf{r}}'|} \exp\left[-\int_0^{|\bar{\mathbf{r}} - \bar{\mathbf{r}}'|} \Sigma_t\left(\bar{\mathbf{r}} - s \frac{\bar{\mathbf{r}} - \bar{\mathbf{r}}'}{|\bar{\mathbf{r}} - \bar{\mathbf{r}}'|}, E \right) ds \right] \delta\left(\hat{\mathbf{\Omega}} \cdot \frac{\bar{\mathbf{r}} - \bar{\mathbf{r}}'}{|\bar{\mathbf{r}} - \bar{\mathbf{r}}'|} - 1 \right) \end{aligned} \tag{2.4e}$$

$$\tilde{S}(\mathbf{P}) = \int d\mathbf{P} S(\bar{\mathbf{r}}'', E, \hat{\mathbf{\Omega}}, t) T(E, \hat{\mathbf{\Omega}}, t; \bar{\mathbf{r}}'' \to \bar{\mathbf{r}}) \tag{2.4f}$$

Eqs. (2.4b), (2.4c), (2.4d), (2.4e) and (2.4f) represent the collision density, transport kernel, collision kernel, transition kernel and the first collision density of source respectively. ν_r is the average number of neutrons produced from reaction type *r*, f_r is probability that a collision of type *r* by a neutron

direction $\hat{\mathbf{\Omega}}'$ and energy E' will produce a neutron in direction interval $d\hat{\mathbf{\Omega}}$ about $\hat{\mathbf{\Omega}}$ with energy *dE* about *E* and *S* is source distribution [24].

After reviewing Neumann series solution, the neutron density tally at the end of m^{th} time step can be calculated as;

$$N_m(\mathbf{r},t) = \frac{1}{N}\left(f_{m-1} \sum_{i=1}^{N} \sum_{j} w_{i,j} q_{i,j} \right) \tag{2.5}$$

where f_{m-1} is a scale factor introduced at the end of $(m\text{-}1)^{th}$ time step, $w_{i,j}$ is weight of neutron after the j^{th} collision of neutron *i* and $q_{i,j}$ is response of neutron density tally for the j^{th} collision of neutron *i*.

2.2.1 Definition of Scale Factor

In order to obtain the desired neutron density level, a scale factor is introduced. It is defined as the sequence based on the ratio of the number of neutrons survived at the time boundary to the number of neutron histories gives the next term as a function of previous term. Mathematically, the scale factor at the m^{th} time step can be written as;

$$f_m = f_{m-1} . \frac{n_{s_m}}{N}; \quad m = 1, 2, 3, \ldots \tag{2.6}$$

where n_{s_m} and N are the number of survival neutrons and the number of neutron histories at the end of m^{th} time step respectively.

2.2.2 Recursive Formulation of Scale Factor

Consider the initial value of scale factor as;

$$n_{s_0} = N \Rightarrow f_0 = 1$$

From Eq. (3), one can obtain;

$$f_1 = f_0\left(\frac{n_{s_1}}{N}\right)$$

$$f_2 = f_1\left(\frac{n_{s_2}}{N}\right) = f^0\left(\frac{n_{s_1}}{N}\right)\left(\frac{n_{s_2}}{N}\right)$$

$$f_3 = f_2\left(\frac{n_{s_3}}{N}\right) = f^0\left(\frac{n_{s_1}}{N}\right)\left(\frac{n_{s_2}}{N}\right)\left(\frac{n_{s_3}}{N}\right)$$

$$\vdots$$

$$f_m = f_{m-1}\left(\frac{n_{s_m}}{N}\right) = f^0\left(\frac{n_{s_1}}{N}\right)\left(\frac{n_{s_2}}{N}\right)\left(\frac{n_{s_3}}{N}\right)\cdots\left(\frac{n_{s_m}}{N}\right) = f_0\prod_{k=1}^{m}\left(\frac{n_{s_k}}{N^k}\right)$$

A recursive formulation for the scale factor by using the preceding term to define the next term of the sequence can be written as;

$$f_m = \prod_{k=0}^{m}\left(\frac{n_{s_k}}{N^k}\right) \tag{2.7}$$

By substituting the value of scale factor from Eq. (2.7) into Eq. (2.5), the neutron density tally can be rewritten as;

$$N_m(\mathbf{r},t)=\frac{1}{N}\left(\prod_{k=0}^{m-1}\left(\frac{n_{s_k}}{N^k}\right)\cdot\sum_{i=1}^{n_m}\sum_{j}w_{i,j}q_{i,j}\right) \tag{2.8}$$

The objective of the introduction of scaling factor is to change the level of neutron density to the desired amount in super-critical reactors. There is no time information with the neutrons simulated in the Monte Carlo criticality calculations. However, it is needed to save the time information to describe the time-dependent behavior of neutrons, so that time mark is introduced in the TDMC algorithm. In Figure 2.2, t_0 denotes the start time of the time-dependent simulation, t_m represents the time boundary, i.e., time cut-off. $f_0, f_1, f_2,.., f_{m-1}$ are calculated at the end of each time bin. For neutron density tally f_0 contributes to the time step interval $t_0 \sim t_1$, f_1 contributes to the time bin $t_1 \sim t_2$, and f_{m-1} contributes to the time bin $t_{m-1} \sim t_m$.

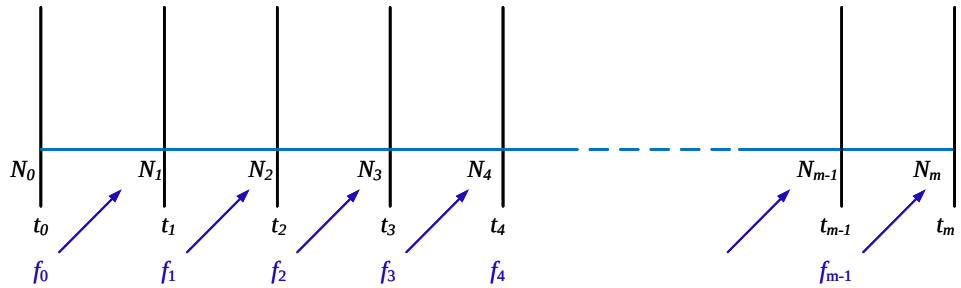

Figure 2.2: Time-dependent neutron density tally

2.3 Estimation of Prompt Neutron Decay Constant Alpha

The neutron Boltzmann equation under certain assumptions that the neutron transport through time independent media, and initially, without considering the effect of delayed neutrons, can be written as;

$$\begin{aligned}&\frac{1}{\upsilon(E)}\frac{\partial}{\partial t}\phi(\mathbf{r},E,\mathbf{\Omega},t)+\mathbf{\Omega}\cdot\nabla\phi(\mathbf{r},E,\mathbf{\Omega},t)+\sum_t(\mathbf{r},E)\phi(\mathbf{r},E,\mathbf{\Omega},t)\\&=\int_0^\infty\int_{4\pi}\sum_s(\mathbf{r},E'\to E,\mathbf{\Omega}'\to\mathbf{\Omega})\phi(\mathbf{r},E',\mathbf{\Omega}',t)d\mathbf{\Omega}'dE'\\&+\frac{\chi_p(\mathbf{r},E)}{4\pi}\int_0^\infty\int_{4\pi}\nu_p\sum_f(\mathbf{r},E')\phi(\mathbf{r},E',\mathbf{\Omega}',t)d\mathbf{\Omega}'dE'+S\end{aligned}\tag{2.9}$$

where $\phi(\mathbf{r},E,\mathbf{\Omega},t)$ is neutron flux, $S(\mathbf{r},E,\mathbf{\Omega},t)$ is flux independent source, $\sum_t(\mathbf{r},E)$, $\sum_f(\mathbf{r},E)$ and $\sum_s(\mathbf{r},E)$ are total cross section, fission cross section and scattering cross section respectively, ν_p is the average number of propmt neutrons emitted per fission and $\upsilon(E)$ is the neutron speed.

In terms of neutron density rather than neutron flux, the Eq. (2.9) becomes;

$$\begin{aligned}&\frac{\partial N(\mathbf{r},E,\mathbf{\Omega},t)}{\partial t}+\mathbf{\Omega}\cdot\nabla\left(\upsilon.N(\mathbf{r},E,\mathbf{\Omega},t)\right)+\sum_t(\mathbf{r},E)\left(\upsilon.N(\mathbf{r},E,\mathbf{\Omega},t)\right)\\&=\int_0^\infty\int_{4\pi}\sum_s(\mathbf{r},E'\to E,\mathbf{\Omega}'\to\mathbf{\Omega})\left(\upsilon.N(\mathbf{r},E,\mathbf{\Omega},t)\right)d\mathbf{\Omega}'dE'\\&+\frac{\chi_p(\mathbf{r},E)}{4\pi}\int_0^\infty\int_{4\pi}\nu_p\sum_f(\mathbf{r},E')\left(\upsilon.N(\mathbf{r},E,\mathbf{\Omega},t)\right)d\mathbf{\Omega}'dE'+S\end{aligned}\tag{2.10}$$

To derive the time dependent fundamental mode solution for true analog criticality calculation, it is assumed that there is no source term, the media for neutron transport is considered to be infinite and integrate over space, energy and direction to obtain the equation;

$$\frac{dN}{dt} + \Sigma_t \left(\upsilon.N\right) = \Sigma_s \left(\upsilon N\right) + \nu_p \Sigma_f \left(\upsilon N\right) \tag{2.11}$$

$$\Rightarrow \quad \frac{dN}{dt} = \left(\nu_p \Sigma_f - \left(\Sigma_t - \Sigma_s\right)\right)\left(\upsilon.N\right)$$

$$\Rightarrow \quad \frac{dN}{dt} = \upsilon\left(\nu_p \Sigma_f - \Sigma_a\right) N$$

Rearranging the terms will give;

$$\frac{dN}{dt} = \upsilon\Sigma_a \left(\frac{\nu_p \Sigma_f}{\Sigma_a} - 1\right) N \tag{2.12}$$

$$\Rightarrow \frac{dN}{dt} = \left(\frac{K-1}{L}\right) N; \quad K = \frac{<\nu>\Sigma_f}{\Sigma_a}; \qquad L = \frac{1}{\upsilon\Sigma_a} \tag{2.12a}$$

where K is the neutron multiplication factor and L is the neutron lifetime.

The initial value problem to be solved for 1D, 1G problem becomes;

$$\frac{dN}{dt} = \alpha N; \quad N(t) = N(t_0) = N_0 \ \ at \ t_0 = 0 \tag{2.13}$$

where $\alpha = \dfrac{K-1}{L}$

Solution to the above differential equation becomes;

$$\frac{1}{N}\frac{dN}{dt} = \frac{d}{dt}\left[\ln N\right] = \alpha \tag{2.14}$$

$$\Rightarrow \quad N(t) = N(t_0)Exp(\alpha * t)$$

$$\Rightarrow \quad \alpha = \frac{\ln\left(N(t)/N(t_0)\right)}{t} \tag{2.15}$$

The prompt neutron decay constant α_m at the end of each m^{th} time boundary is estimated by the mathematical expression given in Eq. 13;

$$\alpha_m = \frac{\ln\left(N(t_m)/N(t_{m-1})\right)}{\Delta t_m}; \quad \Delta t_m = t_m - t_{m-1} \tag{2.16}$$

2.4 Numerical Results

To investigate the effectiveness of TDMC module implemented for the estimation of α eigenvalue in the McCARD, it is applied to the rod model, the infinite homogeneous two group problems and the experimental benchmarks performed on the thorium-loaded accelerator-driven system (Th-ADS).

2.4.1 The Rod Model

Figure 2.3 represents a rod model, which is a simplest example of transport problem. It is considered a time-dependent neutron transport through time independent media, i.e., there is no change in material with time through which neutron is transporting. An infinite homogeneous and isotropic media in which neutrons move at constant speed υ along the line (the rod) and undergo collision events at a rate $v\Sigma$.

Table 2.1 shows one group cross-sections for infinite homogeneous super critical system with $k_\infty = 1.875$. Table 2.2 shows the comparisons of the results for the α eigenvalues using TDMC simulations for 10,000 neutron histories and 500 time steps with 50 inactive time steps with those from the analytical solution. The time step size for the TDMC simulations is set to 1.0 ns. It is observed that the results are in good agreement with the analytical solution.

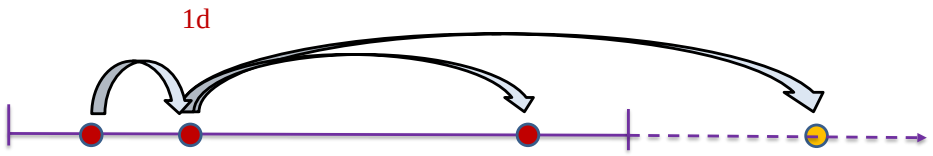

Figure 2.3: Neutron transport through one dimensional infinite homogeneous media

Table 2.1: One group cross-sections for infinite homogeneous super critical system

ν	Σ_f	Σ_a	Σ_s	$1/\upsilon$ [sec/cm]
2.5	0.3	0.4	0.2	1.02245×10^{-9}

Table 2.2: Comparisons of α estimates for the one-group infinite homogeneous problem

Analytical Alpha	Alpha by TDMC (SD)	Relative Error [%]
-3.05639E+7	-3.05745E+7 (0.0057)	0.035

2.4.2 Numerical Results for Infinite Homogeneous Two-Group Problems

Two-group infinite homogeneous medium problems are used to investigate the effectiveness of TDMC module implemented in the McCARD. Table 2.3 represents the two-group cross sections varying the prompt subcriticality k_p with the differential scattering cross section of the fast group Σ_{s12}.

Table 2.4 shows the variation of differential scattering cross section along with the values of k_p. Table 2.5 shows the comparisons of the results for the α eigenvalues using TDMC simulations for 10,000 neutron histories and 500 time steps with 50 inactive time steps with those from the reference, the α iteration algorithm [3] and the *α-k* iteration method applying the pseudo absorption adjustment [10] with analytical solutions. The time bin size for the DMC simulations is set to 1.0 μs for each prompt criticality. It is observed that the results are within 95% confidence intervals. Figure 2.4 shows the convergence of α eigenvalue using the TDMC simulations for different k_p values.

Table 2.3: Cross sections for the two-group infinite homogeneous problem [3]

Cross Section	First group (g=1)	Second group (g=2)
Σ_{tg}	0.5	0.5
Σ_{fg}	0.025	0.175
ν_{pg}	2.0	2.0
Σ_{sgg}	0.10	0.20
$\Sigma_{sg'g}$ $(g \neq g')$	Variable	0.00
χ_{pg}	1.0	0.0
$1/\upsilon_g$ [sec/cm]	2.28626×10^{-10}	1.29329×10^{-6}

Table 2.4: Prompt criticality k_p with the varying differential scattering cross section of the first group [3]

Σ_{s12}	k_p
0.265714	0.9
0.197143	0.7
0.128571	0.5
0.060000	0.3
0.008571	0.15

Table 2.5: Comparisons of α estimates for the two-group infinite homogeneous problem

k_p	Ref. α	α-k iteration with η = 0 (SD)	α-k iteration with η = 2 (SD)	α iteration (SD)	α using DMC (SD)
0.90	26507.1	26500.1 (12.8)	26545.6 (14.8)	26524.4 (14.0)	26511.2 (49.3)
0.70	79523.4	79574.6 (33.8)	79455.7 (38.7)	79522.6 (18.0)	79532.2 (80.4)
0.50	132544.0	132518.0 (70.8)	132431.0 (94.4)	132539.0 (20.9)	132501.0 (94.1)
0.30	185568.0	Fail	Fail	185554.0 (26.6)	185542.0 (120.4)
0.15	225338.0	Fail	Fail	225328.0 (31.3)	225227.0 (147.2)

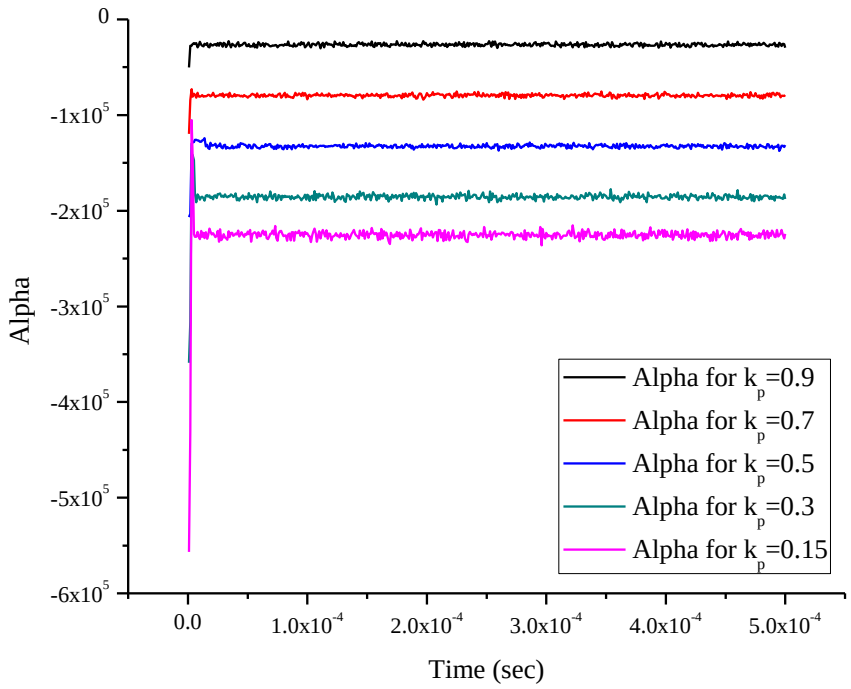

Figure 2.4: Convergence of alpha using TDMC simulations for different k_p values

2.4.3 Application to Th-ADS Experimental Benchmarks

The TDMC algorithm is applied to calculate the α eigenvalue for the experimental benchmarks performed on the thorium-loaded accelerator-driven system (Th-ADS). The solid-moderated and solid-reflected type A core of KUCA facility is used to perform Th-ADS experiments. Seven core configurations are combined with the accelerator, generating the 14 MeV pulsed neutrons by D-T (deuteron-tritium) reactions or a synchrotron type proton accelerator. The highly enriched uranium (HEU), thorium (Th), and natural uranium (NU) fuel was loaded together with the reflectors, including polyethylene (PE), graphite (Gr), and beryllium (Be) [7].

Figure 2.5(a) represents a core configuration for Th-PE, Th-Gr, Th-Be, Th-HEU-PE, and NU-PE cores with 3 He detectors and Figure 2.5(b) shows a core configuration for Th-HEU-5PE and Th-HEU-Gr-PE cores with 2 He detectors having accelerator generating 14 MeV pulsed neutrons. The effective multiplication factors, k_{eff}'s, of all the cores are shown in the Table 2.6.

Table 2.6: k_{eff}*'s* of the seven core configurations

Core	k_{eff}
Th-PE	0.00613
Th-Gr	0.00952
Th-Be	0.00765
Th-HEU-PE	0.58754
NU-PE	0.50867
Th-HEU-5PE	0.85121
Th-HEU-Gr-PE	0.35473

The McCARD calculations along with the TDMC module are performed with continuous-energy cross section libraries produced from the ENDF/B-VII.0 for all the cores. The results for the α eigenvalues using TDMC simulations for 10,000 neutron histories and 250 time steps with 50 inactive time steps are shown in the Table 2.7. The time bin size for the TDMC simulations is set to 0.1 ms for each core. From the comparisons with the measurements, the MC PNS simulations and the MC α iteration show that the α eigenvalue measured by the TDMC method are quite comparable and it is observed that the results are within 95% confidence intervals. Figure 2.6(a) and Figure 2.6(b) show the neutron flux distribution with time for Th-Gr and Th-HEU-5PE cores respectively. Figure 2.7(a) and Figure 2.7(b) represent

the convergence of the α from TDMC simulations for Th-Gr and Th-HEU-5PE cores respectively.

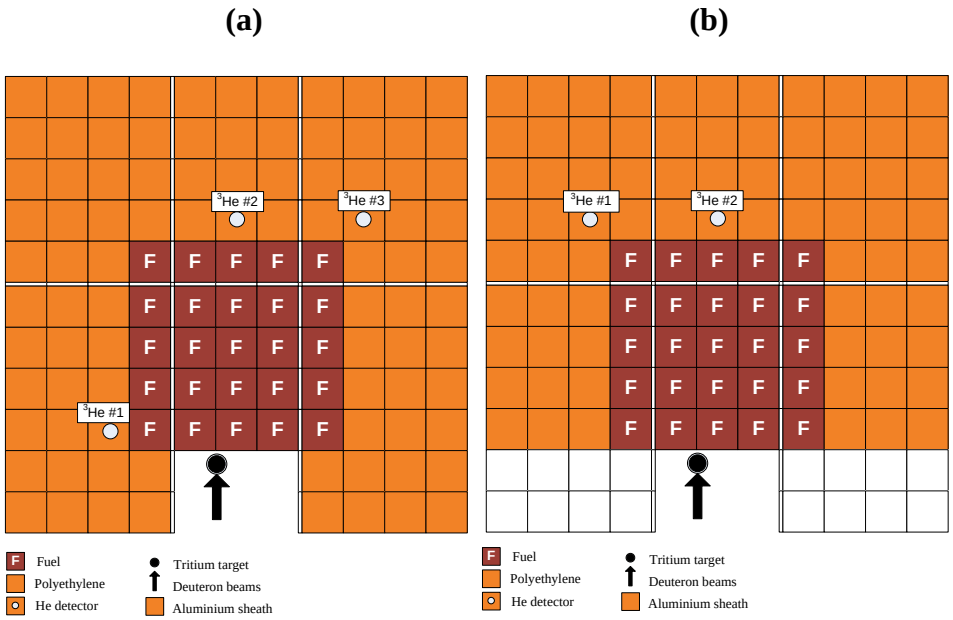

Figure 2.5: Core configurations with 14 MeV pulsed neutrons for Th-ADS experimental benchmarks. (a). Th-PE, Th-Gr, Th-Be, Th-HEU-PE, and NU-PE (b). Th-HEU-5PE and Th-HEU-Gr-PE

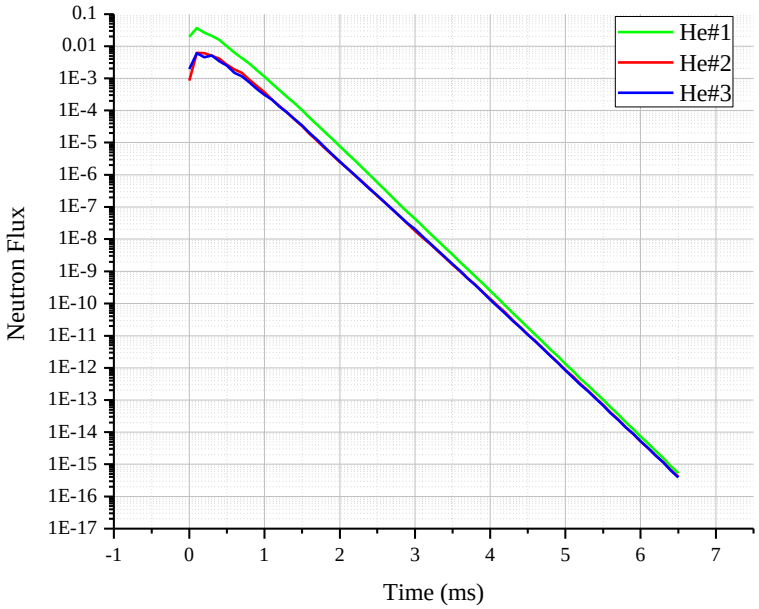

(a) Th-Gr Core

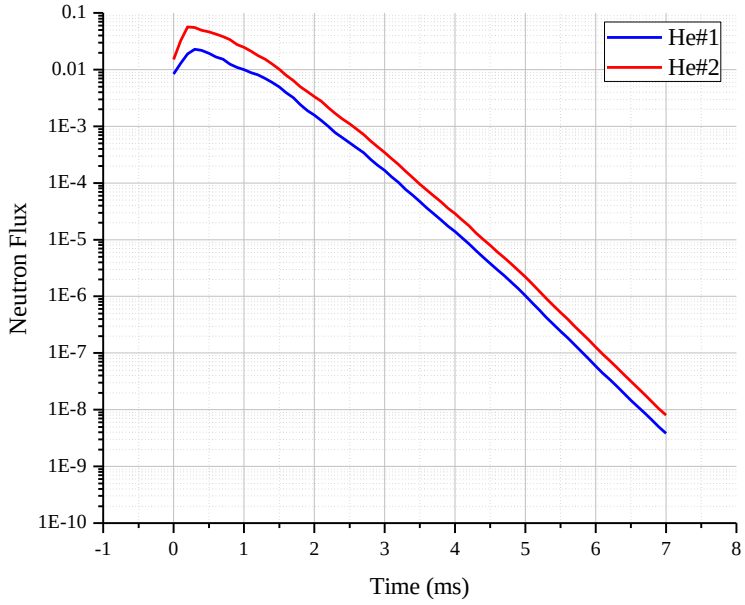

(b) Th-HEU-5PE Core

Figure 2.6: TDMC neutron flux for the Th-ADS benchmark problems

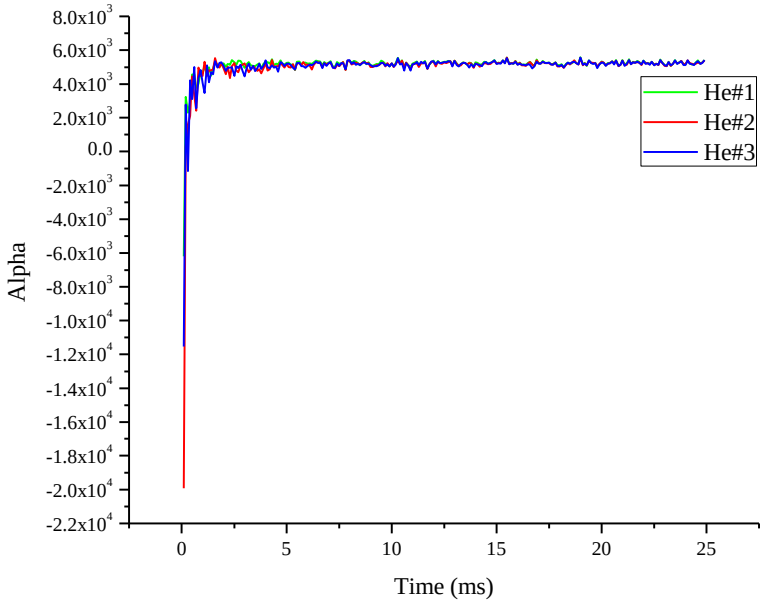

(a) Th-Gr Core

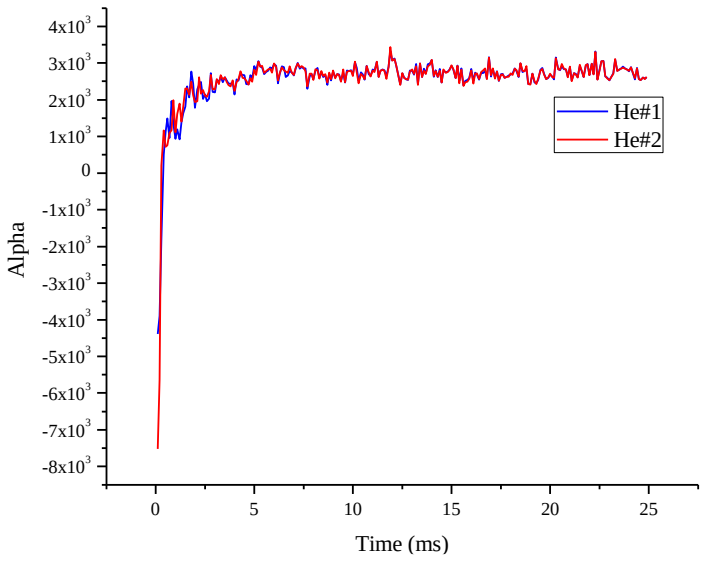

(b) Th-HEU-5PE Core

Figure 2.7: Convergence of alpha using TDMC simulations for the Th-ADS benchmark problems

Table 2.7: Comparison of the α eigenvalues for the Th-ADS experimental benchmarks

CORE	Measurement with 14 MeV neutrons (SD)			MC PNS Simulation (SD)	MC α iteration (SD)	α using TDMC (SD) [Rel. Diff. (%)]			Mean α Rel. Diff. [%] (w/PNS Sim.) [w/α iteration]
	^{3}HE #1	^{3}HE #2	^{3}HE #3			^{3}HE #1	^{3}HE #2	^{3}HE #3	
TH-PE	6642 (11)	6224 (27)	5751 (25)	5245.4 (4.9)	5243.3 (1.3)	5240.9 (8.7) [21.1]	5196.1 (9.3) [16.5]	5177.0 (9.8) [10.0]	5204.6 (0.8) [0.7]
TH-GR	6451 (12)	5945 (15)	5701 (17)	5310.1 (7.7)	5239.7 (1.3)	5233.5 (8.3) [18.9]	5193.2 (8.6) [12.6]	5190.0 (9.1) [9.0]	5205.5 (2.0) [0.7]
TH-BE	6515 (8)	6111 (17)	5746 (20)	5224.2 (7.2)	5240.1 (1.4)	5223.6 (9.2) [19.8]	5148.3 (9.5) [15.8]	5186.4 (9.5) [9.7]	5198.1 (0.5) [0.8]
TH-HEU-PE	5692 (11)	5275 (7)	5231 (9)	5025.6 (6.3)	5131.2 (2.8)	5051.3 (10.1) [11.3]	5027.7 (10.4) [4.7]	5015.8 (10.8) [4.1]	5031.6 (0.1) [1.9]
NU-PE	5748 (11)	6592 (15)	5010 (11)	4995.1 (6.4)	5163.8 (3.5)	5106.3 (9.7) [11.2]	5065.8 (11.0) [23.2]	5053.7 (11.1) [0.9]	5075.3 (1.6) [1.7]
TH-HEU-5PE	3110 (11)	3104 (10)	--	2977.1 (1.4)	2954.1 (1.2)	2905.6 (12.3) [11.7]	2895.1 (12.4) [11.6]	--	2900.3 (7.8) [7.1]
TH-HEU-GR-PE	4980 (40)	4939 (50)	--	4761.0 (2.9)	4766.7 (10.2)	4772.8 (9.6) [5.2]	4779.5 (9.1) [5.2]	--	4776.1 (0.3) [0.2]

CHAPTER. 3 The Time-Dependent Monte Carlo Algorithm for the Transient Analysis of Nuclear Reactors

3.1 Coupled System of Equations for Transient Analysis of Nuclear Reactor

For the transient analysis of nuclear reactors, coupled system of equations must be solved. The coupled system of time-dependent neutron Boltzmann transport equation with the delayed neutron precursor concentrations can be written as;

$$\begin{aligned}&\frac{1}{\upsilon(E)}\frac{\partial}{\partial t}\phi(\mathbf{r},E,\mathbf{\Omega},t)+\mathbf{\Omega}\cdot\nabla\phi(\mathbf{r},E,\mathbf{\Omega},t)+\Sigma_t(\mathbf{r},E)\phi(\mathbf{r},E,\mathbf{\Omega},t)\\&=\frac{\chi_p(E)}{4\pi}\int_0^\infty\int_{4\pi}\left(1-\beta(\mathbf{r},E')\right)\nu(\mathbf{r},E')\Sigma_f(\mathbf{r},E')\phi(\mathbf{r},E',\mathbf{\Omega}',t)\,d\mathbf{\Omega}'dE'\\&\int_0^\infty\int_{4\pi}\Sigma_s(\mathbf{r},E'\to E,\mathbf{\Omega}'\to\mathbf{\Omega})\phi(\mathbf{r},E',\mathbf{\Omega}',t)\,d\mathbf{\Omega}'dE'+S_d(\mathbf{r},E,\mathbf{\Omega},t)+S(\mathbf{r},E,\mathbf{\Omega},t)\end{aligned}\tag{3.1}$$

$$\frac{\partial}{\partial t}C_i(\mathbf{r},t)=\int_0^\infty\int_{4\pi}\beta_i(\mathbf{r},E')\nu(\mathbf{r},E')\Sigma_f(\mathbf{r},E')\phi(\mathbf{r},E',\mathbf{\Omega}',t)d\mathbf{\Omega}'dE'-\lambda_iC_i(\mathbf{r},t)\tag{3.2}$$

$$S_d(\mathbf{r},E,\mathbf{\Omega},t)=\frac{1}{4\pi}\sum_i\lambda_iC_i(\mathbf{r},t)\chi_i(E)\tag{3.3}$$

In the above equations,

ϕ = neutron flux,

$\Sigma_t(\mathbf{r}, E')$ = total cross-section,

$\Sigma_s(\mathbf{r}, E')$ = differential scattering cross-section,

$\Sigma_f(\mathbf{r}, E')$ = fission cross-section,

$\chi_p(E)$ = spectrum of prompt fission neutrons,

$\chi_i(E)$= spectrum of the i^{th} group of delayed fission neutrons,

$\beta(\mathbf{r}, E')$ = total delayed neutron fraction and $\beta(\mathbf{r}, E') = \sum_i \beta_i(\mathbf{r}, E')$,

$\beta_i(\mathbf{r}, E')$ = delayed neutron fraction of the i^{th} group of delayed neutrons,

ν = average neutron yield at fission,

$C_i(\mathbf{r}, t)$ = precursor concentration of delayed neutrons in i^{th} group,

λ_i = decay constant of family i,

S_d = delayed neutron source,

S = external source.

All quantities in Eqs. (3.1), (3.2) and (3.3) are dependent on either space, directions, energy, or time, but most are dependent on a combination of these variables. In fact, the neutron flux is seven-dimensional, which makes these equations difficult to discretize.

The Monte Carlo method is an efficient method to solve such multidimensional equations.

3.2 TDMC Steady-State Simulation

Because we apply existing methods for the delayed neutron generation [1] and the neutron population control [12] in this TDMC transient study, a new MC steady-state calculation method based on the TDMC tracking is focused on in this section.

The main difference between the TDMC simulation and the MC eigenvalue calculation [19] is that the former is applying the exact collision kernel, C, at each collision site while the latter the scattering collision kernel, C_s, which are defined by;

$$C(\mathbf{r}';E',\mathbf{\Omega}'\to E,\mathbf{\Omega})=\sum_r \nu_r(\mathbf{r}',E')\cdot\frac{\Sigma_r(\mathbf{r}',E')}{\Sigma_t(\mathbf{r}',E')}\cdot f_r(E',\mathbf{\Omega}'\to E,\mathbf{\Omega}) \quad (3.4)$$

$$C_s(\mathbf{r}';E',\mathbf{\Omega}'\to E,\mathbf{\Omega})=\sum_{r\neq fis.} \nu_r(\mathbf{r}',E')\cdot\frac{\Sigma_r(\mathbf{r}',E')}{\Sigma_t(\mathbf{r}',E')}\cdot f_r(E',\mathbf{\Omega}'\to E,\mathbf{\Omega}) \quad (3.5)$$

ν_r is the average number of neutrons produced from a reaction type r and $f_r(E',\mathbf{\Omega}'\to E,\mathbf{\Omega})dEd\mathbf{\Omega}$ is the probability that a collision of type r by a neutron of direction $\mathbf{\Omega}'$ and energy E' will produce a neutron in direction interval $d\mathbf{\Omega}$ about $\mathbf{\Omega}$ with energy in dE about E. Other notations

follow standard. By comparing Eqs. (3.4) and (3.5), the only difference is whether the fission reaction is sampled or not. The fission reaction can be sampled in the reaction-type sampling process of the TDMC method like the MC fixed-source-mode calculations while it is discarded in the MC power iteration method. Then the ignored fission reaction in the reaction-type sampling process is considered by sampling fission source neutrons for the next iteration (or generation) MC simulations with probability of $w \cdot \left(\frac{\nu_f(\mathbf{r}', E')}{k} \right) \cdot \left(\frac{\Sigma_f(\mathbf{r}', E')}{\Sigma_t(\mathbf{r}', E')} \right)$ where w, ν_f, and k are the neutron weight, the average number of total fission neutrons per a fission at the collision site, and the fundamental-mode k eigenvalue, respectively. In this MC power iteration algorithm, the division by k in the fission neutron production probability plays the role of source normalization iteration-by-iteration (or generation-by-generation). And as well-known [22,23], this replacement of ν_f by a fictitious one, $\nu_{fic.}$ defined by ν_f / k, is the only alteration of the eigenvalue equation for the steady-state analysis from the physical system.

By making the best of the concept of $\nu_{fic.}$, fundamental-mode distributions of fission sources and delayed neutron precursors as well as

k can be obtained via TDMC simulations with slight modification. Suppose that a total number of time steps, a step interval, a number of neutron histories and an initial k value are provided in a user input for the TDMC steady-state calculations.

In this TDMC simulation with the population control, the only modification to obtain the fundamental-mode distributions of fission sources and delayed neutron precursors is to generate fission neutrons as many as ν_f^m / k_{i-1}, where ν_f^m and $k_{i\text{-}1}$ are the average number of total fission neutrons of isotope m and the eigenvalue estimated at the time step (i-1), when a fission reaction of isotope m is selected during the MC simulations. From each time step TDMC simulations, k can be estimated by calculating a ratio between amounts of the fission neutron productions and the net losses of neutrons.

Then after the modified TDMC simulations for the user-provided number of time steps which is supposed to enough to converge the fission source distribution, initial fission sources for the MC transient simulation are determined as survived neutrons at the end of this TDMC steady-state calculations. Initial sites of the delayed neutron precursors are

selected with the probability of $w \cdot \nu_d(\mathbf{r}', E') \cdot \left(\frac{\Sigma_f(\mathbf{r}', E')}{\Sigma_t(\mathbf{r}', E')} \right)$, where ν_d is the number of delayed neutrons per fission, at every collision site during the last time step TDMC simulations with applying the population control technique of the delayed neutron precursors [1].

Figure 3.1 shows an algorithm of the TDMC steady-state calculations at the i^{th} time step. In the figure, $SNB_{i'}$ (i' =i or i-1) means a data structure storing survived neutrons at time $T_{i'+1}$.

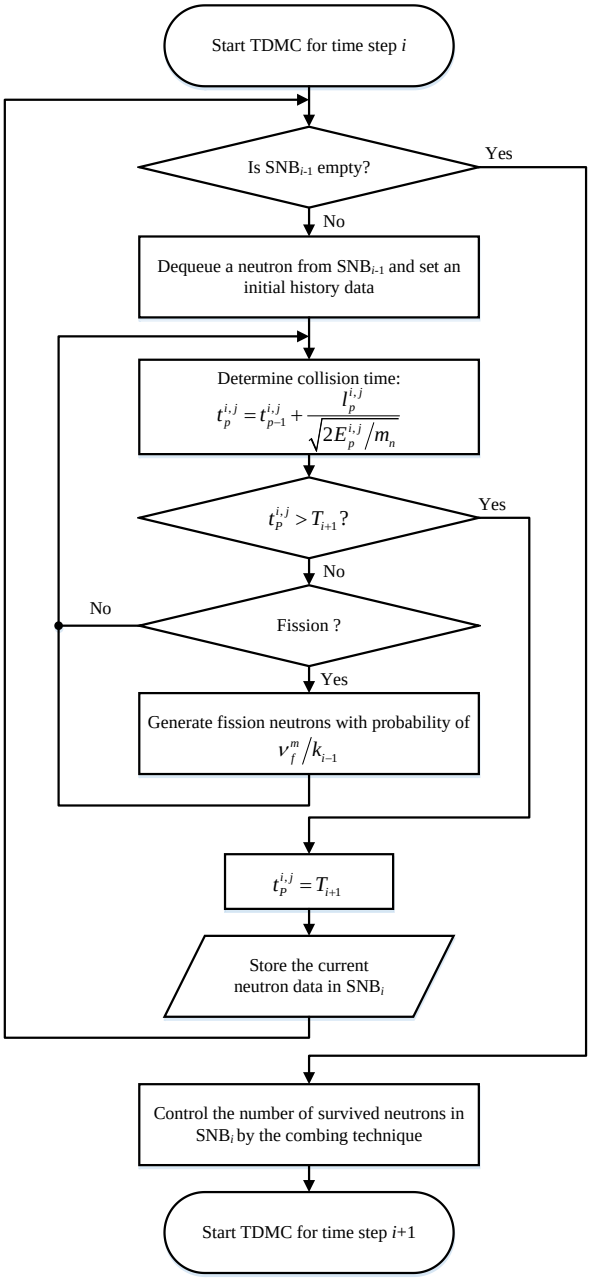

Figure 3.1: Flow chart of the TDMC steady-state calculation at time step *i*

3.3 Numerical Results for the Transient Analysis without Temperature Feedback for the OECD/NEA C5G7-TD Benchmark

3.3.1 C5G7-TD Application Results

The C5G7-TD benchmark [20] specifies a series of space-time neutron kinetics problems without consideration of any feedback effects for the verification of transient analysis codes. The C5G7-TD benchmark problems are based on the well-studied steady-state C5G7 specification [24] and additionally defines physical constants related to delayed neutron characteristics. Its two-dimensional (2D) core configuration is the same as the C5G7 core consisting of sixteen fuel assemblies (FAs), eight UO_2 FAs and eight mixed oxide (MOX) FAs, as shown in Figure 3.2. Each 17x17 FA has 264 fuel pins, 24 guide tubes (GTs) for control rods (CRs) and one instrument tube (IT) for a fission chamber (FC) in the center grid-cell. Every pin cell with pitch of 1.26 cm is modeled by two regions – a cylinder with radius 0.54 cm for a mixture region of fuel-clad, moderator-filled GT, CR-GT, or FC-IT and a surrounding moderator region. There are four CR banks each of which governs CRs

in FAs at the same position in the quarter symmetry. Bank numbers of 1, 2, 3, and 4 are assigned for north-west, north-east, south-west, and south-east FAs, respectively, in Figure 3.2.

The C5G7-TD benchmark provides four exercise sets from 0 to 3 on the 2D configuration and two exercise sets of 4 and 5 on a 3D geometry. Transient events in the 2D problem sets can be modeled by time-dependent changes of the seven-group macroscopic cross sections in the CR-GT mixture regions. In this paper, McCARD DMC calculation results for the four 2D problem sets are presented and verified via comparisons with those calculated by a deterministic code, nTRACER [21]. The McCARD DMC calculations for the 2D benchmark problems are performed from 0 s to 3 s with time intervals of 0.05 ms using 100,000 neutron histories.

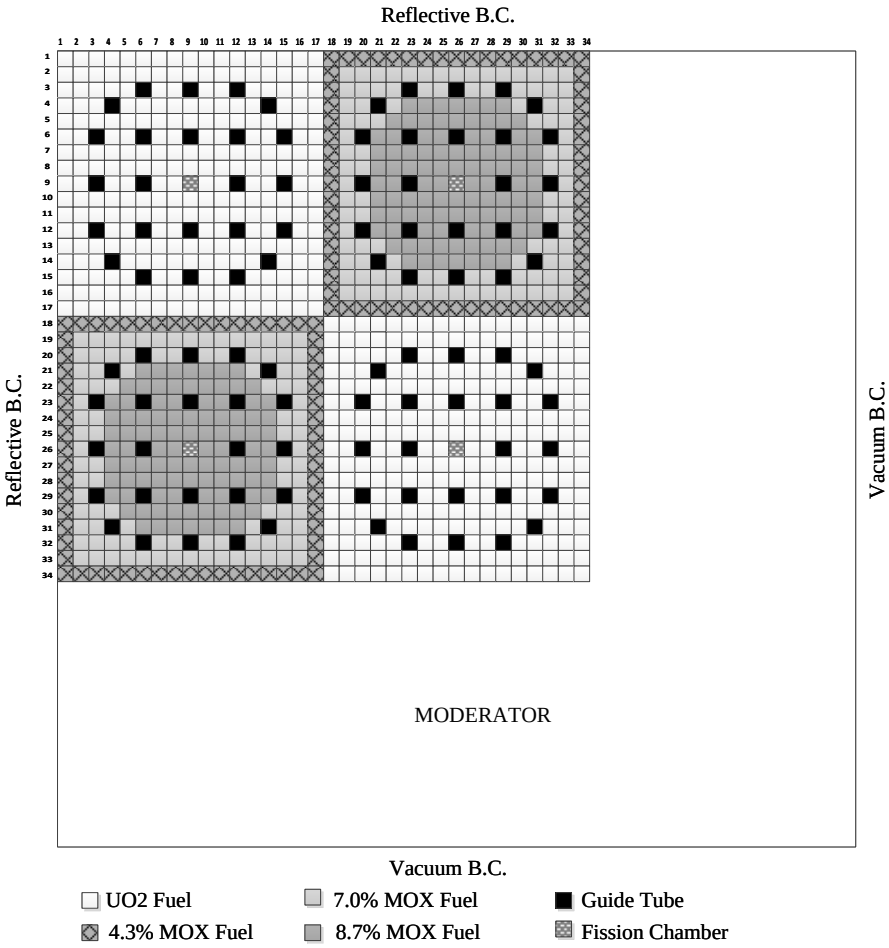

Figure 3.2: 2D core configuration for the C5G7-TD benchmark

3.3.2 TDMC Steady-State Calculation

The TDMC steady-state simulation is newly proposed to generate initial prompt neutron sources and delayed neutron precursors for the MC transient simulation. In order to investigate the effect of the time step interval, the TDMC steady-state calculations during 200 time steps are performed with varying the interval as 0.0001, 0.001, 0.01, 0.05, 0.1, 1.0, and 2.5 ms considering that the prompt neutron generation time is estimated to be about 0.014 ms by the MC adjoint-weighted kinetics parameter estimation method [17]. Figure 3.3 shows convergence plots of the fundamental-mode eigenvalue or k_{eff} by the TDMC steady-state simulations with changing the step interval. From the figure, one can see that k_{eff} becomes converged after 50 time steps. Figure 3.4 shows the comparison of converged k_{eff}'s calculated by averaging the estimated k_{eff} values from 51^{st} to 200^{th} time step with a reference calculated from the standard MC eigenvalue calculations method [19]. The error bars in Figure 3.4 indicates the ±2 standard deviation (SD) intervals of the mean values where the SDs are calculated by the square root of the sample variance from the time step-wise k_{eff} values of the TDMC steady-state calculations while the gray area from the cycle-wise k_{eff} estimates in the

MC eigenvalue calculation. From the figure, one can see that the mean estimate of k_{eff} by the TDMC steady-state calculations agrees well with the MC eigenvalue calculation result. This can be assured by the comparisons of flux spectra in the TDMC steady-state calculations with that of the MC eigenvalue calculation shown in the Figure 3.5. From these results, it is concluded that the TDMC steady-state calculations can be conducted for any time step interval. In this study, the TDMC steady-state calculations are performed by choosing step interval 0.05 ms with 200 time steps for 100,000 histories.

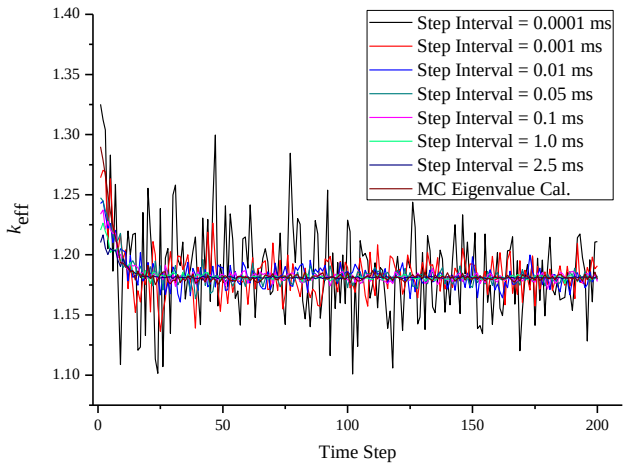

Figure 3.3: k_{eff} convergence plots of the TDMC steady-state calculations for 2D C5G7-TD with varying the time step intervals as 0.0001, 0.001, 0.01, 0.05, 0.1, 1.0 and 2.5 ms

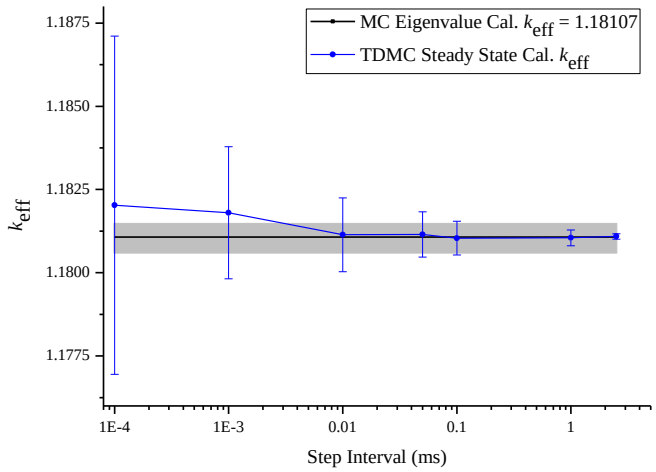

Figure 3.4: Comparison of converged k_{eff} values calculated by the TDMC steady-state simulations for 2D C5G7-TD according to the time step interval

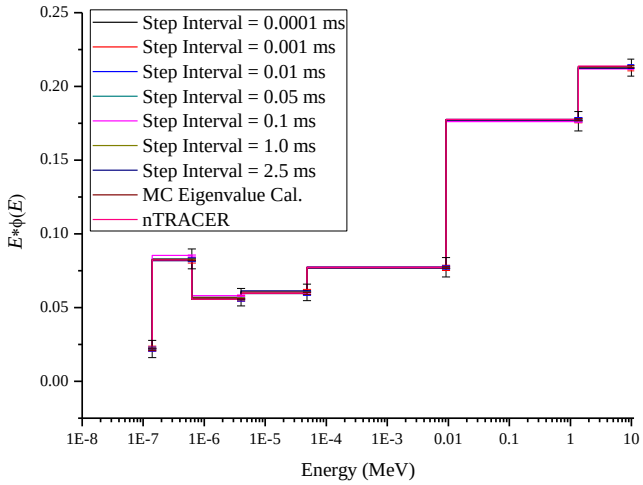

Figure 3.5: Comparison of flux spectra with varying the time step interval in the TDMC steady-state simulations for the 2D C5G7-TD core

3.3.3 2-D Transient Problems

3.3.3.1 C5G7 Exercise 0 (TD0)

In the problem set TD0, a postulated instantaneous CR insertion and withdrawal transient of designated CR banks is modeled by step changes of the cross sections of the GT mixture regions, Σ^{GTM}, during 2 s as;

$$\Sigma_{rg}^{GTM}(t)=\begin{cases}\Sigma_{rg}^{GT};\ t=0,\ t\geq 2\text{ s}\\ \Sigma_{rg}^{GT}+0.1\left(\Sigma_{rg}^{R}-\Sigma_{rg}^{GT}\right);\ 0\text{ s}<t\leq 1\text{ s}\\ \Sigma_{rg}^{GT}+0.05\left(\Sigma_{rg}^{R}-\Sigma_{rg}^{GT}\right);\ 1\text{ s}\leq t<2\text{ s}\end{cases} \tag{3.9}$$

where *r* and *g* are the reaction type and energy group indices, respectively. The superscripts *GT* and *R* represent the moderator-filled *GT* and the *CR-GT* composition, respectively.

Among five problems in TD0, the McCARD TDMC calculations are performed for TD0-1 and TD0-5 where the postulated CR movements of bank 1 and all the banks, respectively, occur. Figure 3.6 shows comparisons of the core dynamic reactivity calculated by McCARD and nTRACER for problems TD0-1 and TD0-5. From Figure 3.6(a), one can observe abrupt decreases of reactivity at 0 s by sudden

insertion of CRs, constant reactivities until 1 s, sudden increases at 1 s by moving the CRs to half position of the inserted length, and restorations at 2 s by withdrawing the CRs to the initial positions. Figure 3.6(b) magnifies the comparisons in a range between 0.1 s and 0.5 s with the ±2 SD intervals of the mean estimates over the tally interval of 2.5 ms, where the SD is calculated by the sample SD from the history-wise estimates during each 2.5 ms. Figure 3.7 shows comparisons of fractional total core fission rates, defined by the fraction of the total core fission rate to its initial value at 0 s, calculated by McCARD and nTRACER for problems TD0-1 and TD0-5. From the figures, one can see that the McCARD TDMC calculation results agree well with nTRACER's.

(a) 0 s ≤ t ≤ 3 s

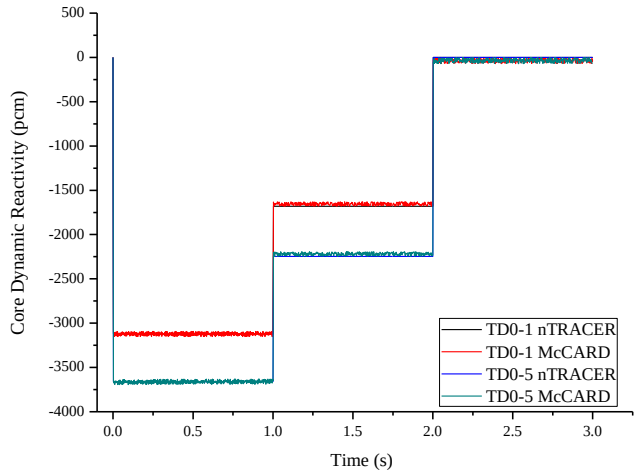

(b) 0.1 s ≤ *t* ≤ 0.5 s

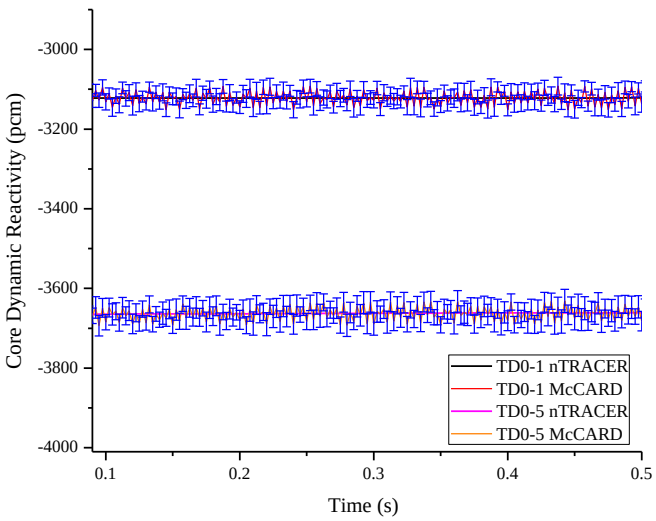

Figure 3.6: Comparisons of dynamic reactivities calculated by McCARD and nTRACER for problems TD0-1 and TD0-5

(a) 0 s ≤ t ≤ 3 s

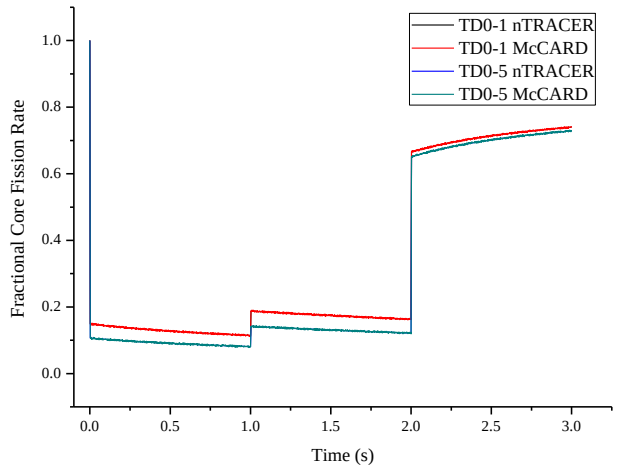

(b) 0.1 s ≤ t ≤ 0.5 s

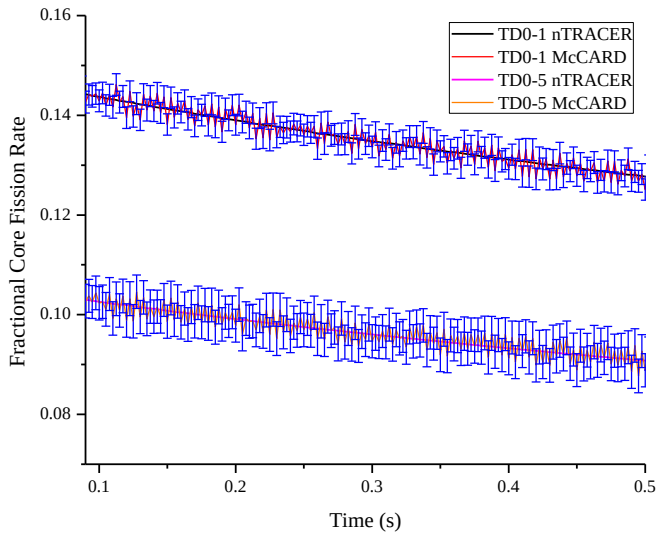

Figure 3.7: Comparisons of fractional total fission rates calculated by McCARD and nTRACER for problems TD0-1 and TD0-5

3.3.3.2 C5G7 Exercises 1 and 2 (TD1 and TD2)

Exercises 1 and 2 (TD1 and TD2, respectively) represents core transients due to CR insertion and extraction at a constant speed. In both problem sets, the cross sections of the GT region are defined by

$$\Sigma_{rg}^{GTM}(t)=\begin{cases}\Sigma_x^{GT}+\alpha\left(\Sigma_x^R-\Sigma_x^{GT}\right)t;\ 0\ \text{s}\le t<1\ \text{s}\\ \Sigma_{rg}^{GT}+\alpha\left(\Sigma_x^R-\Sigma_x^{GT}\right)\left(2-t\right);\ 1\ \text{s}\le t<2\ \text{s}\\ \Sigma_{rg}^{GT};\ t\ge 2\ \text{s}\end{cases} \tag{3.10}$$

where α is the cross section change rate, whose value is 0.01 for TD1 and 0.1 for TD2. Figures 3.8 and 3.9 show comparisons of dynamic reactivities and the fractional total fission rates, respectively, calculated by McCARD and nTRACER for TD1-1 and TD2-1 with considering the CR movements in bank 1. From Figure 3.8, one can observe that reactivity linearly decreases from 0 s to 1 s and increases after 1 s until 2 s due to ramp changes of cross sections at the GT regions by Eq. (3.10). From the figures, one can see that the McCARD TDMC calculation results agree well with nTRACER's as the cases of TD0-1 and TD0-5.

(a) 0 s ≤ t ≤ 3 s

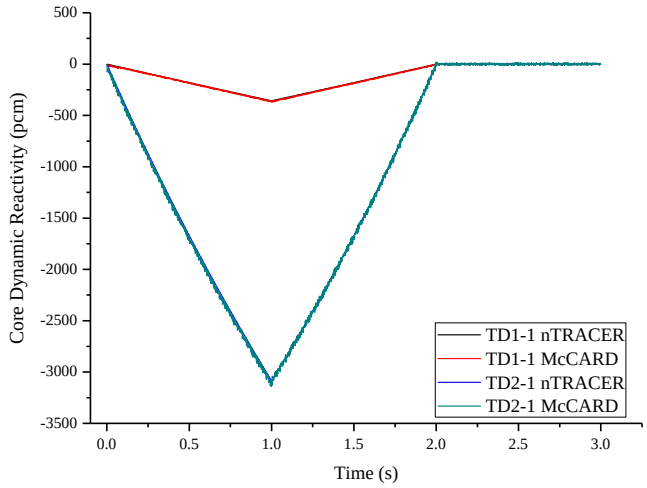

(b) 0.1 s ≤ t ≤ 0.5 s

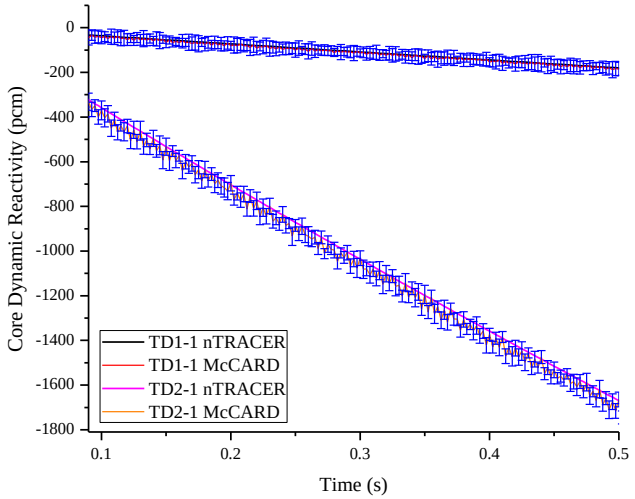

Figure 3.8: Comparisons of dynamic reactivities calculated by McCARD and nTRACER for problems TD1-1 and TD2-1

(a) 0 s ≤ t ≤ 3 s

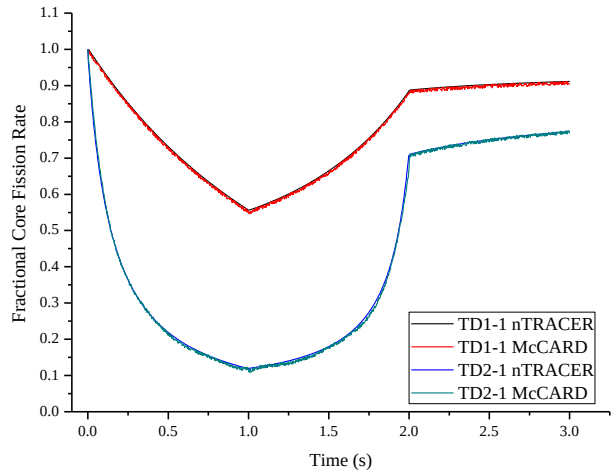

(b) 0.1 s ≤ t ≤ 0.5 s

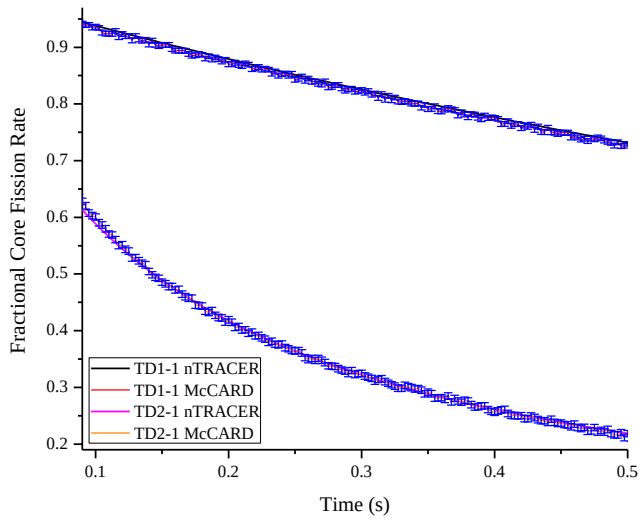

Figure 3.9: Comparisons of fractional total fission rates calculated by McCARD and nTRACER for problems TD1-1 and TD2-1

3.3.3.3 C5G7 Exercise 3 (TD3)

The Exercise 3 (TD3) is designed for a transient event of the change in the core moderator density. Figure 3.10 illustrates four scenarios of the time-dependent fraction changes of the moderator density. According to the density change profile, the time-dependent cross sections of moderator, Σ^{M3}, in each TD3 problem can be expressed as;

$$\Sigma_{rg}^{M3}(t) = \begin{cases} \Sigma_{rg}^{M} - (1-\omega)\Sigma_{rg}^{M} t; \ 0 \text{ s} \le t < 1 \text{ s} \\ (2\omega - 1)\Sigma_{rg}^{M} + (1-\omega)\Sigma_{rg}^{M} t; \ 1 \text{ s} \le t < 2 \text{ s} \\ \Sigma_{rg}^{M}; \ \ t \ge 2 \text{ s} \end{cases} \tag{3.11}$$

where ω is the minimum change fraction of which values are 0.95, 0.90, 0.85, and 0.80 for TD3-1, TD3-2, TD3-3, and TD3-4 cases, respectively. The superscripts M indicates moderator.

Figures 3.11 and 3.12 show comparisons of dynamic reactivities and the fractional total fission rates, respectively, calculated by McCARD and nTRACER for TD3 problems with changing ω. Figure 3.11 illustrates that linear decreases of reactivities during the first 1 s and their linear increases for next 1 s because of moderator densities linear changes shown in Figure 3.10. From the figures, it is demonstrated that the McCARD TDMC calculation results agree well with nTRACER's.

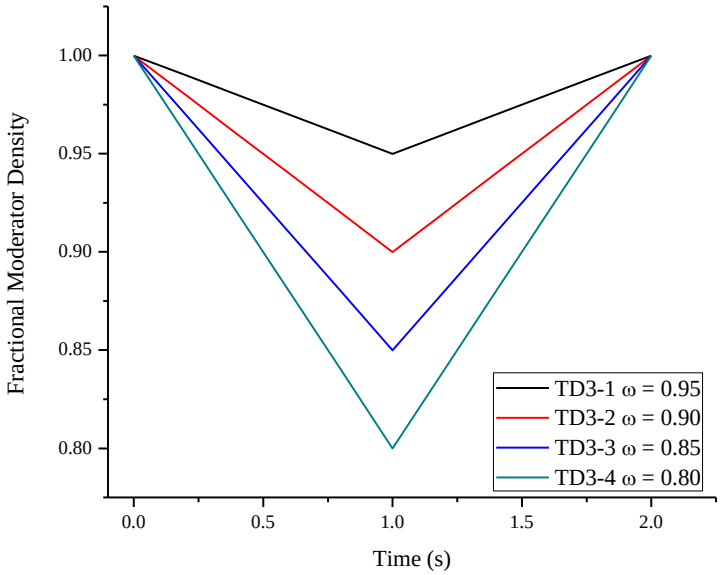

Figure 3.10: Core moderator density changes in the TD3 problems

(a) 0 s ≤ t ≤ 3 s

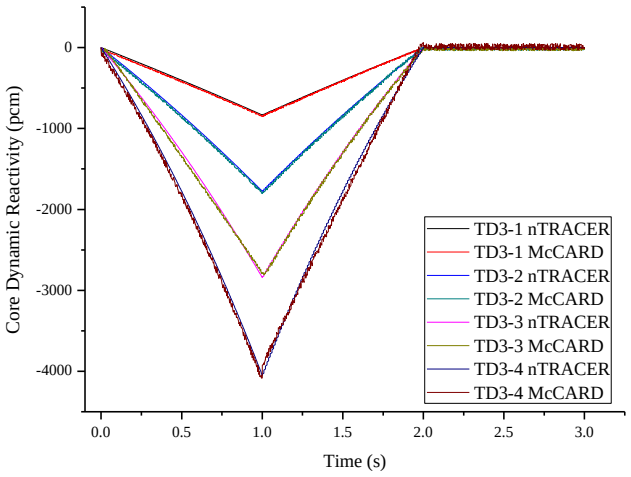

(b) 0.1 s ≤ t ≤ 0.5 s

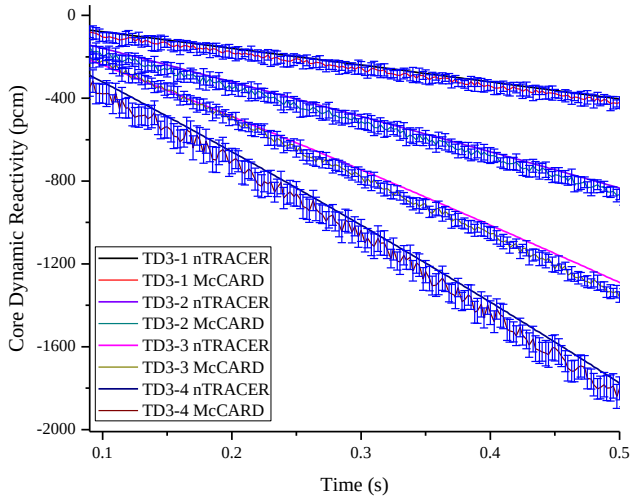

Figure 3.11: Comparisons of dynamic reactivities calculated by McCARD and nTRACER for the TD3 problems

(a) 0 s ≤ t ≤ 3 s

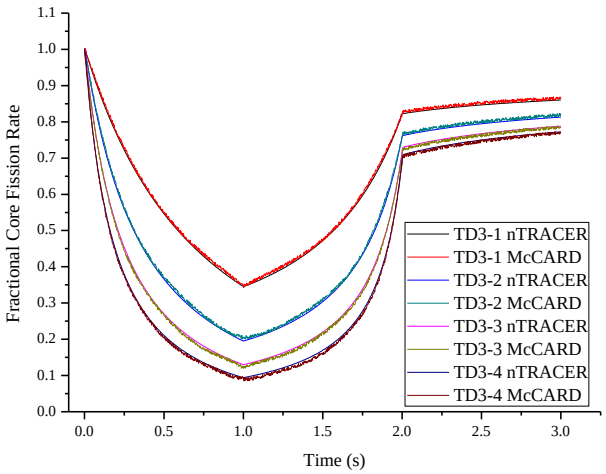

(b) 0.1 s ≤ t ≤ 0.5 s

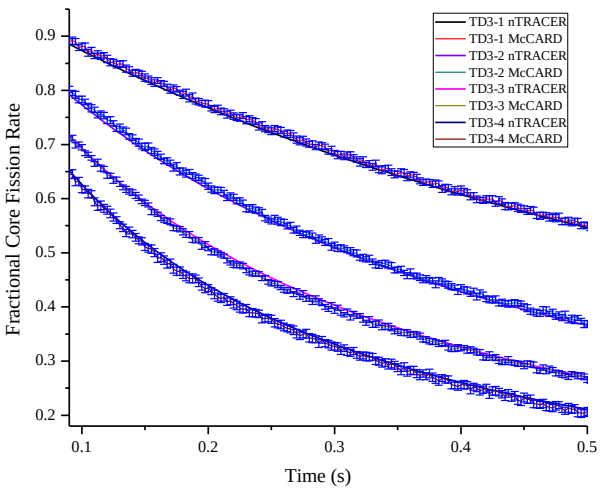

Figure 3.12: Comparisons of fractional total fission rates calculated by McCARD and nTRACER for the TD3 problems

3.3.4 3-D Transient Problems

3.3.4.1 C5G7 Exercise 4 (TD4)

Exercises 4 (TD4) represents core transients due to CR insertion and extraction in 3-D core configuration. It is assumed that the rod bank moves at a constant speed, which allows it to be fully inserted into the assembly from the fully withdrawn position within 6 s. This hypothetic value is proposed only for the purpose of reducing the computational effort in the transient calculation. Among five problems in TD4, the McCARD TDMC calculations are performed for TD4-1 and TD4-5 where the postulated CR movements of bank 1 and bank 1 & bank 3, respectively, occur. Figure 3.13 illustrates the corresponding scenarios of the time-dependent fractional rod bank insertion and extraction for TD4-1 and TD4-5 problems.

Figures 3.14, 3.15, 3.16 and 3.17 show comparisons of dynamic reactivities and the fractional total fission rates, respectively, calculated by McCARD and nTRACER for TD4-1 and TD4-5. From the figures, one can see that the McCARD TDMC calculation results agree well with nTRACER's results.

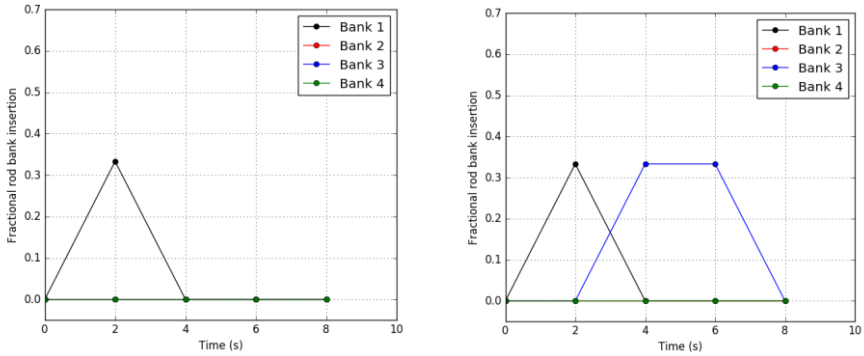

Figure 3.13: Relative depth of control bank movement in TD4-1 and TD4-5 problems

(a) 0 s ≤ t ≤ 6 s

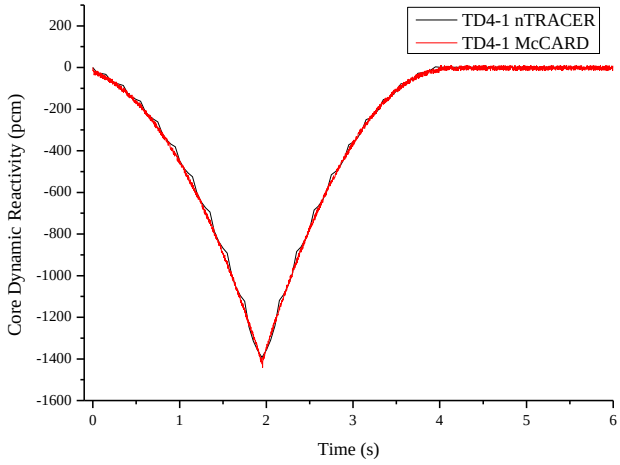

(b) 0 s ≤ t ≤ 0.5 s

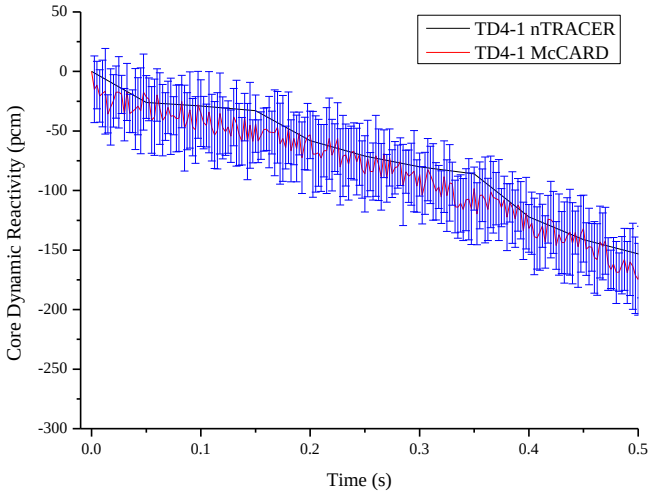

Figure 3.14: Comparisons of dynamic reactivities calculated by McCARD and nTRACER for TD4-1 problem

(a) 0 s ≤ t ≤ 10 s

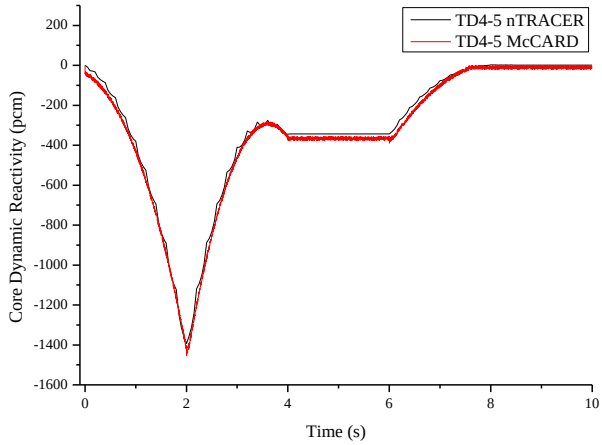

(b) 0 s ≤ t ≤ 0.5 s

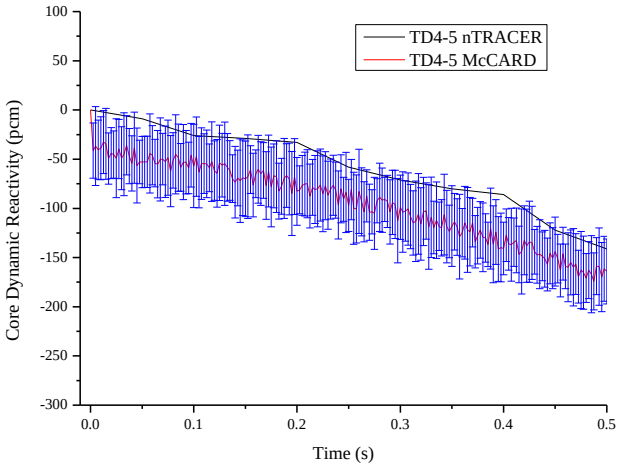

Figure 3.15: Comparisons of dynamic reactivities calculated by McCARD and nTRACER for TD4-5 problem

(a) 0 s ≤ t ≤ 6 s

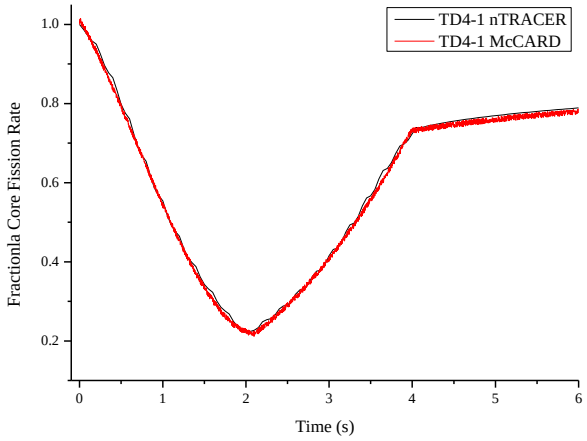

(b) 0 s ≤ t ≤ 0.5 s

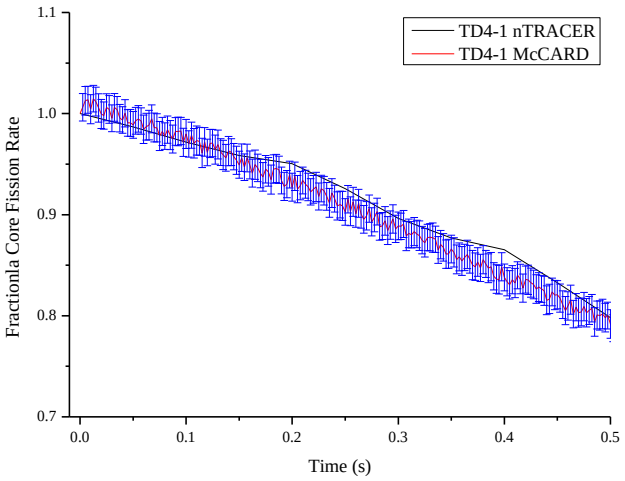

Figure 3.16: Comparisons of fractional total fission rates calculated by McCARD and nTRACER for TD4-1 problem

(a) 0 s ≤ t ≤ 10 s

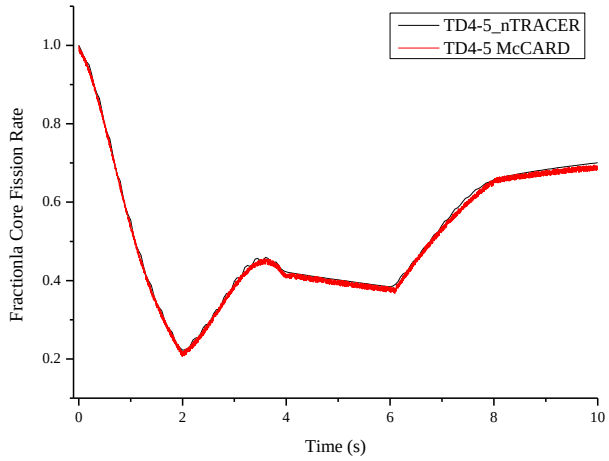

(b) 0 s ≤ t ≤ 0.5 s

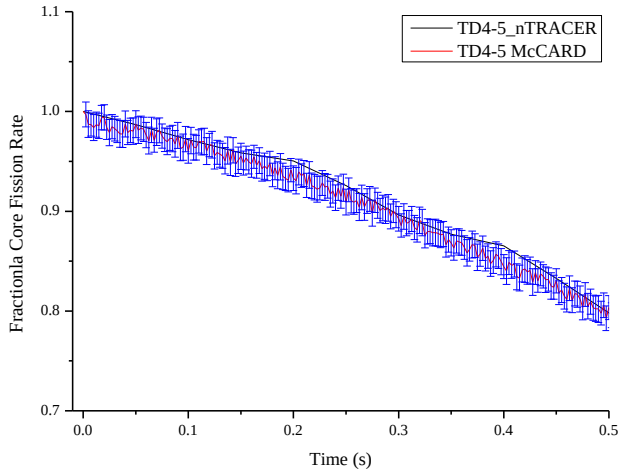

Figure 3.17: Comparisons of fractional total fission rates calculated by McCARD and nTRACER for TD4-5 problem

3.3.4.2 C5G7 Exercise 5 (TD5)

The Exercise 5 (TD3) is intended as a simulation of transient events of the change in the assembly wise moderator density. All the control rods are assumed to be positioned in the fully withdrawn position throughout the transient and initially, the moderator density is considered to be at the nominal level. Figure 3.16 illustrates four scenarios of the time-dependent transient mechanisms by varying the rate and location in the fraction changes of the assembly moderator density. According to the density change profile, the time-dependent cross sections of assembly wise moderator, $\Sigma^{Ma_i 5}$ in each TD5 problem can be expressed as;

$$\Sigma_{rg}^{Ma_i 5}(t) = \begin{cases} \Sigma_{rg}^{Ma_i} - (1-\omega_2)\Sigma_{rg}^{Ma_i} t; & 0\ \text{s} \le t < 1\ \text{s} \\ \begin{cases} (2\omega_2 - \omega_3)\Sigma_{rg}^{Ma_i} - (\omega_2 - \omega_3)\Sigma_{rg}^{Ma_i} t \\ (2-\omega_1)\Sigma_{rg}^{Ma_i} - (1-\omega_1)\Sigma_{rg}^{Ma_i} t \end{cases}; & 1\ \text{s} \le t < 2\ \text{s} \\ \begin{cases} (3\omega_3 - \omega_2)\Sigma_{rg}^{Ma_i} - (\omega_2 - \omega_3)\Sigma_{rg}^{Ma_i} t \\ (3\omega_1 - 2)\Sigma_{rg}^{Ma_i} - (1-\omega_1)\Sigma_{rg}^{Ma_i} t \end{cases}; & 1\ \text{s} \le t < 2\ \text{s} \\ (4\omega_2 - 3)\Sigma_{rg}^{Ma_i} + (1-\omega_2)\Sigma_{rg}^{Ma_i} t; & 3\ \text{s} \le t < 4\ \text{s} \end{cases} \tag{3.9}$$

where ω_1, ω_2 and ω_3 are the minimum change fractions corresponding to the assembly wise moderator density change and $\{a_i;\ i = 1,2,3,4\}$ is the assembly index. The superscripts M indicates moderator. To summarize,

in all the four scenarios in TD5 exercise, the assembly wise ω_1, ω_2 and ω_3 can be defined as;

$$\begin{cases} TD5-1(a_1, a_3): \omega_1 = \omega_2 = 0.95,\ \omega_3 = 0.90 \\ TD5-2(a_1, a_2, a_3): \omega_1 = 0.95,\ \omega_2 = 0.90,\ \omega_3 = 0.80 \\ TD5-3(a_1, a_3, a_4): \omega_1 = 0.95,\ \omega_2 = 0.90,\ \omega_3 = 0.80 \\ TD5-4(a_2, a_3, a_4): \omega_1 = 0.95,\ \omega_2 = 0.90,\ \omega_3 = 0.80 \end{cases}$$

Figures 3.17 and 3.18 show comparisons of dynamic reactivities and the fractional total fission rates, respectively, calculated by McCARD and nTRACER for TD5 problems with changing ω_1, ω_2 and ω_3. From the figures, one can see that the McCARD TDMC calculation results agree well with nTRACER's results.

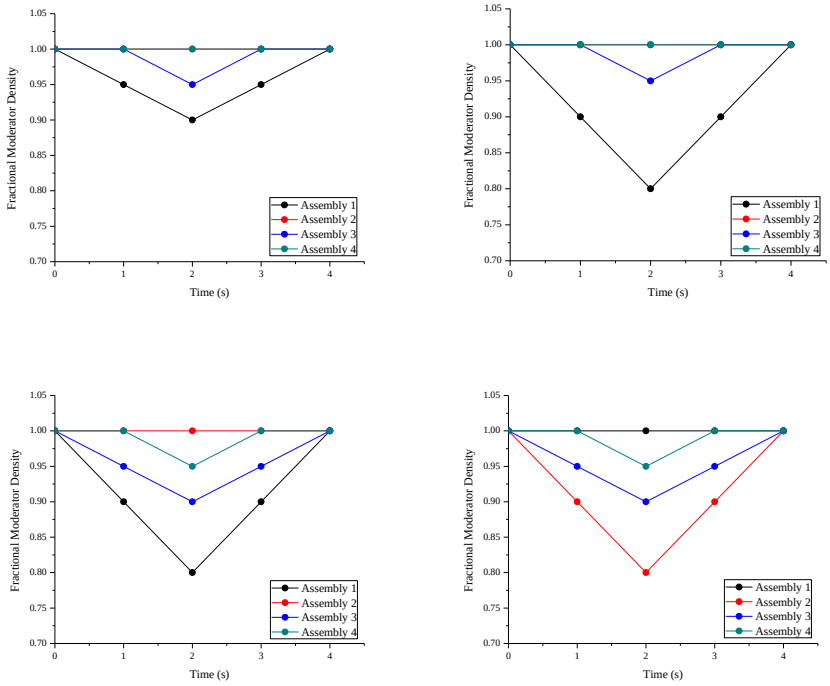

Figure 3.18 Relative moderator density changes in the TD5 problems

(a) 0 s ≤ t ≤ 6 s

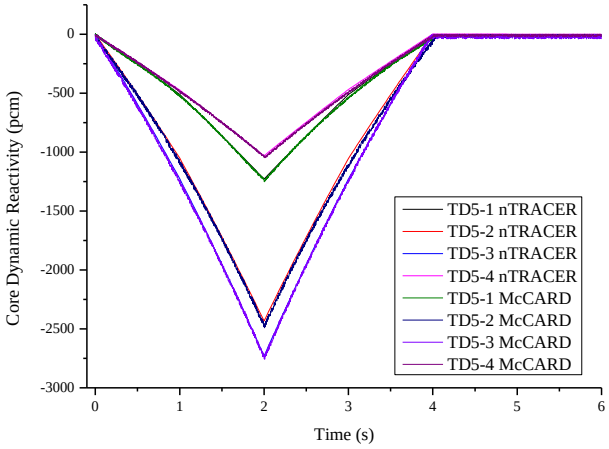

(b) 0 s ≤ t ≤ 0.5 s

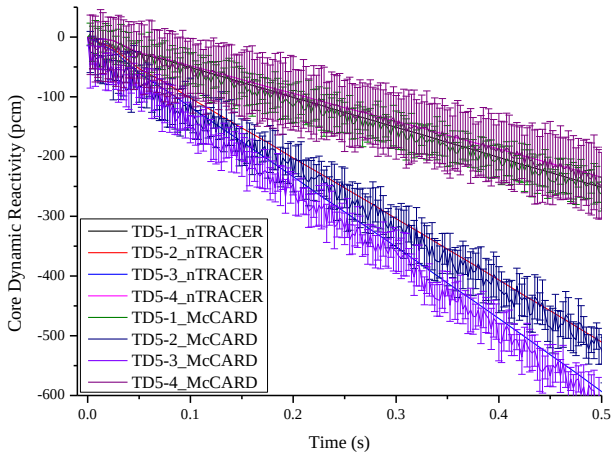

Figure 3.19: Comparisons of dynamic reactivities calculated by McCARD and nTRACER for the TD5 problems

(a) 0 s ≤ t ≤ 6 s

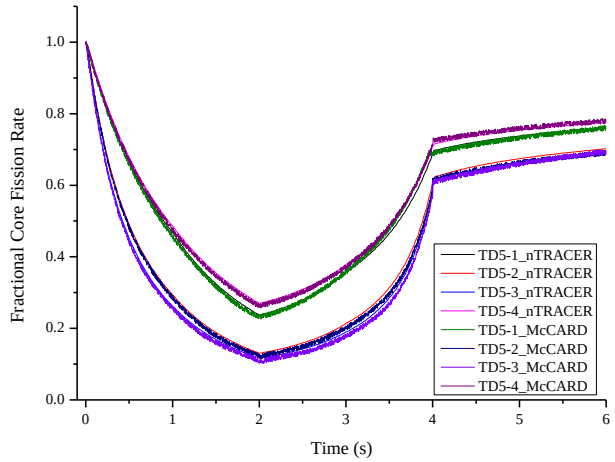

(b) 0 s ≤ t ≤ 0.5 s

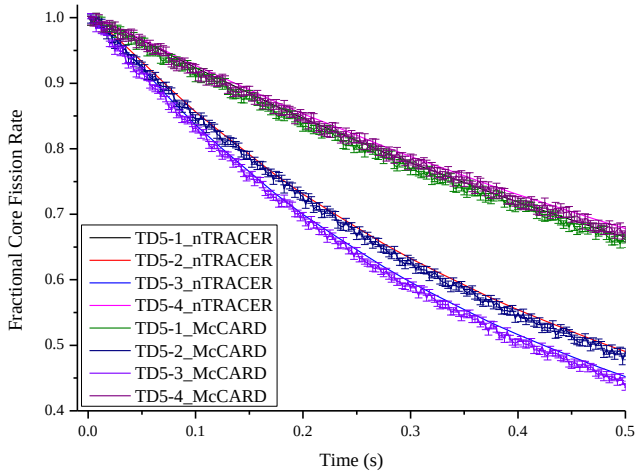

Figure 3.20: Comparisons of fractional total fission rates calculated by McCARD and nTRACER for the TD5 problems

3.4 Numerical Results for the Transient Analysis with Temperature Feedback for the IAEA CRP HTGR UAM Benchmark

In order to do the transient analysis with temperature feedback, the McCARD code is coupled with the CUPID code. The socket communication is used for the explicit coupling of the codes. The McCARD and CUPID codes are connected to a socket server and requested data are transferred to each other through the socket server. The socket server receives and adjusts the data because of different mesh structures between McCARD and CUPID.

Figure 3.21 shows communication scheme between McCARD and CUPID. First, CUPID calculates temperature density profiles from an initially-guessed power profile, while McCARD eigenvalue calculations are conducted to obtain a converged fission source distribution. Then a time-dependent McCARD run starts using the updated temperature and density profiles obtained from CUPID and transfers the updated power profile to CUPID. And CUPID and McCARD calculations are conducted time step-by-step as shown in Figure 3.21.

In this McCARD/CUPID transient calculations, temperature-dependent cross sections are produced by a built-in on-the-fly Doppler broadening (OTF DB) module.

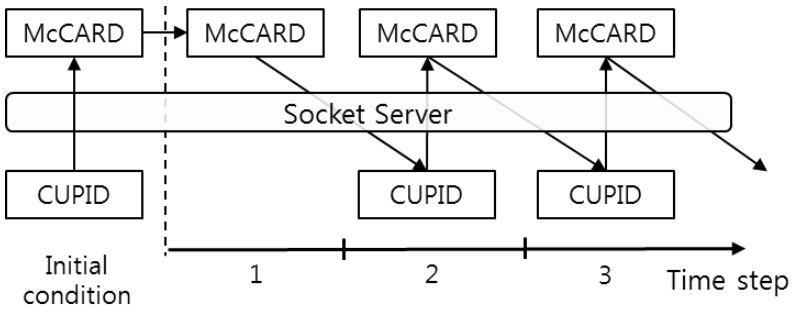

Figure 3.21: Thermal-hydraulics coupling scheme of McCARD/CUPID

3.4.1 IAEA CRP HTGR UAM Benchmark (Triangular Unit Cell Model)

The IAEA CRP HTGR UAM benchmark [25] provides a two-dimensional symmetric 1/12th triangular unit cell model of MHTGR-350 which consists of the UCO fuel compact, helium gap, H-451 graphite and helium coolant channel as shown in Figure 3.22.

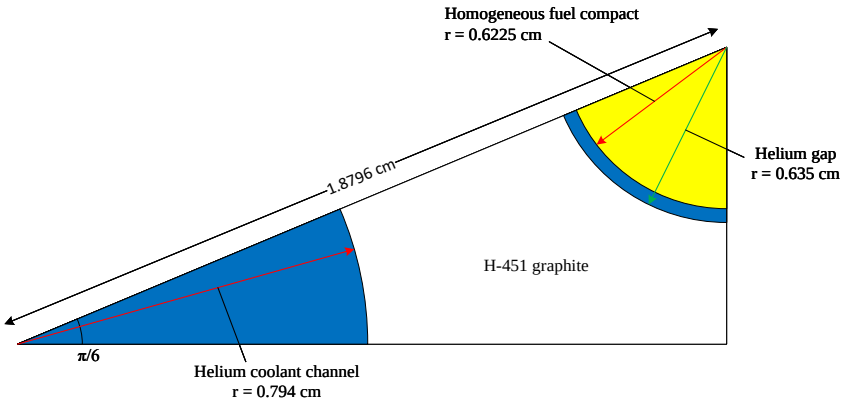

Figure 3.22: Triangular unit cell model

The coolant channel is modelled as a heat sink with bulk temperature of 750 K. Heat is generated in the fuel compact and transferred to H-451 graphite. Boundaries of triangular unit cell are adiabatic condition. All thermo-physical properties are described in Ref. 25. The density of fuel compact, helium gap and H-451 graphite are considered to be a constant, so that there is no density feedback. Number densities are modified by Table 3.1 to set k_{eff} to 1.00850 (0.00009).

Table 3.1: Number densities of nuclides

Nuclide		Number density (atoms/b·cm)
Fuel compact	U-235 U-238 O-16 Graphite Si-28 Si-29 Si-30	1.5803E-05 8.4860E-04 1.5128E-03 7.0132E-02 2.8554E-03 1.4026E-04 8.9769E-05
Coolant channel	He-4	2.4600E-05
H-451 graphite	Graphite	9.2800E-02

3.4.2 Numerical Results

CUPID uses 15,148 hexahedral cells to calculate the temperature profile in the fuel compact, helium gap and H-451 graphite regions. Figure 3.23 shows the temperature profile calculated from the initial condition. McCARD uses single cells for the fuel compact, helium gap and H-451 graphite and average temperatures are assigned to each cell. Average temperature of the fuel compact, gap and H-451 graphite at the initial step are 877.28 K, 853.54 K and 834.03 K, respectively.

The time dependent McCARD calculations are performed with continuous-energy cross section libraries produced from the ENDF/B-VII.0 library. 10,000 neutron histories are simulated per time step. The time step size is set to 10.0 ms. The power density and average temperature of fuel, gap and H-451 graphite over time are shown in Figure 3.24. The power density exponentially increases from 26 MW/m^3 up to 1030.65 MW/m^3 and then decreases drastically by the Doppler feedback effect.

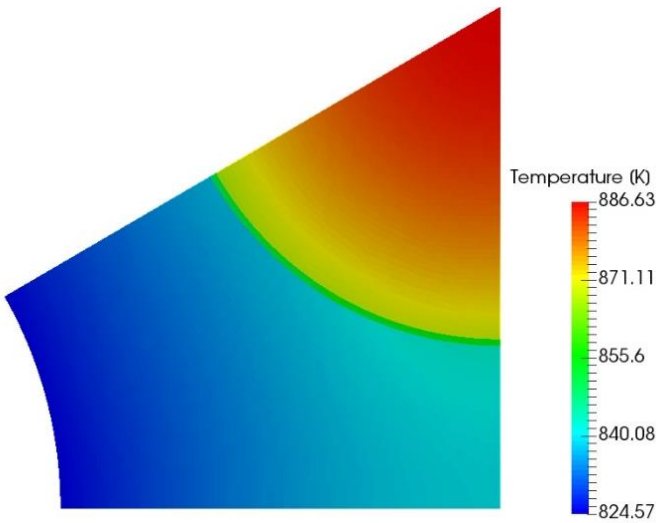

Figure 3.23: Temperature profile at the initial condition

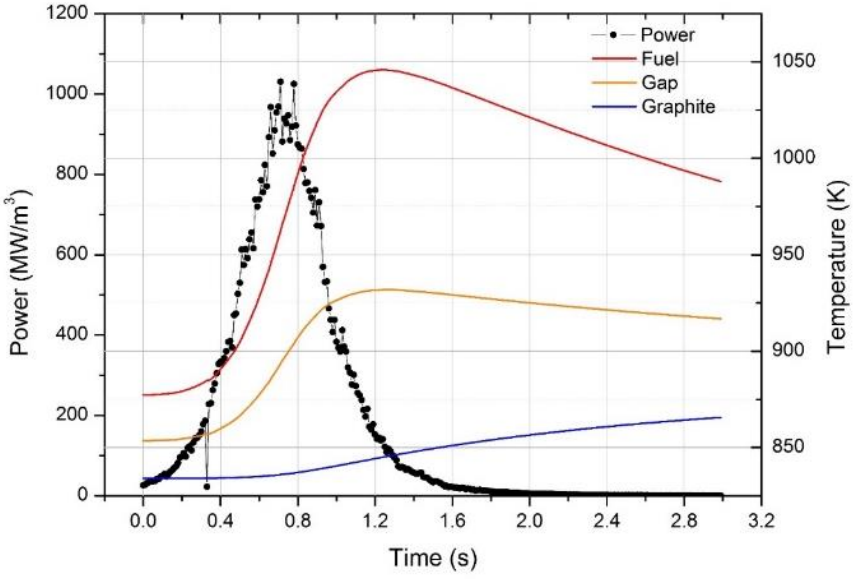

Figure 3.24: Power density and temperature profile

CHAPTER. 4 Uncertainty Propagation Analysis for the Dynamic Monte Carlo Simulations

4.1 Uncertainty Propagation in Neutron Density Tally

The statistical uncertainty of one time step is accumulated with the uncertainty propagating through the calculation from the preceding time step. The main purpose of this chapter is to study this uncertainty propagation at the end of each time boundary. With the help of formal uncertainty propagation approach, it is investigated that how a change in the scale factor at the end of each time boundary affects and propagates the uncertainty in the neutron density of the system. That is a term affected by the propagation of statistical uncertainty in the neutron density from the TDMC simulation [26].

The discussion starts with the uncertainty propagated in scale factor which is a main source of uncertainty in calculating neutron density (N_m) during TDMC calculations and this propagation is continued with the term affected by scale factor (f_{m-1}). Since uncertainty in scale factor further depends on the change in number of survival neutrons (n_{s_k}) at the

end of each time boundary, so the change in the neutron density distribution can be written as;

$$\Delta N_m = \Delta N_m\left(\left\{n_{s_k}\right\}_{k=0}^{m-1}\right) = \frac{1}{N}\left(\prod_{k=0}^{m-1}\left(\frac{n_{s_k}}{N}\right).\sum_{i=1}^{N}\sum_{j} w_{i,j}q_{i,j}\right) \tag{4.1a}$$

Eq. (4.1a) can also be written as;

$$\Delta N_m\left(\left\{n_{s_k}\right\}_{k=0}^{m-1}\right) = \prod_{k=0}^{m-1}\left(\frac{n_{s_k}}{N}\right).A_0 \tag{4.1b}$$

where

$$A_0 = \frac{1}{N}\left(\sum_{i=1}^{N}\sum_{j} w_{i,j}q_{i,j}\right)$$

The formal error propagation approach is to compute standard deviation from the survival neutron components $\left\{n_{s_k}\right\}_{k=0}^{m-1}$ and combine all into standard deviation for scale factor f_{m-1} using the approximation for products of (*m-1*) variables (ignoring the covariance between $\left\{n_{s_k}\right\}_{k=0}^{m-1}$).

The general formulation for uncertainty propagation in absolute units can be written as;

$$S_{N_{m-1}} = N_{m-1}\sqrt{\sum_{k=1}^{m-1}\frac{S_{n_{s_k}}^2}{\left(n_{s_k}\right)^2}}\ ; \qquad m = 2,3,4,... \tag{4.2}$$

In percent units, uncertainty propagation can be written as;

$$\frac{S_{N_{m-1}}}{N_{m-1}} = \sqrt{\sum_{k=1}^{m-1}\frac{S_{n_{s_k}}^2}{\left(n_{s_k}\right)^2}}\ ; \qquad m = 2,3,4,... \tag{4.3}$$

where n_{s_k} represents the number of survival neutrons at the end of k^{th} time step and $S_{n_{s_k}}$ is a standard deviation of survival neutrons at the end of k^{th} time step, calculated as;

$$S_{n_{s_{m-1}}}^2 = \frac{1}{m-2}\left\{\sum_{i=1}^{m-1}\left(n_{s_i}\right)^2 - \frac{\left(\sum_{i=1}^{m-1} n_{s_i}\right)^2}{m-1}\right\} \tag{4.4}$$

In operator notation, Eq. (4.4) can expressed as;

$$e_{N_m} = \left(\frac{S_{N_m}}{N_m}\right)^2 = e_{N_{m-1}} + \varepsilon_{N_m}; \quad \varepsilon_{N_m} = \frac{S_{n_{s_m}}^2}{\left(n_{s_m}\right)^2} \tag{4.5}$$

The repeated application of Eq. (4.5) gives;

$$e_{N_m} = e_{N_0} + \sum_{i=1}^{m}\varepsilon_{N_i} \tag{4.6}$$

4.2 Numerical Results

4.2.1 The Rod Model

The rod model is a simplest example of time-dependent neutron transport through time independent media, i.e., there is no change in material with time through which neutron is transporting. An infinite homogeneous and isotropic media in which neutrons move at constant speed υ along the line (the rod) and undergo collision events at a rate $\nu\Sigma$. A true analog calculation is done for this TDMC simulation without considering the source term S. From Eq. (2.9a),

$$\frac{1}{N}\frac{dN}{dt} = \frac{d\left(\ln N\right)}{dt} = \left[\left(K-1\right)/L\right] \qquad (4.7)$$

The solution of above equation under the assumption that the properties of the medium are time independent is given by;

$$N\left(t\right) = N\left(0\right)\exp\left[\left(K-1\right)/L\right] \qquad (4.8)$$

Table 4.1 shows one-group cross sections for infinite homogeneous super critical system with $k_\infty = 1.875$.

Table 4.1: One-group cross sections for infinite homogeneous problem

ν	Σ_f	Σ_a	Σ_s	$1/\upsilon$ [sec/cm]
2.5	0.3	0.4	0.2	1.02245×10^{-9}

The TDMC neutron density calculations are performed for 10,000 neutron histories and 200 time steps with time step size 1.0 ns. Table 4.2 shows comparisons of neutron density calculated by TDMC algorithm and analytical solutions. From the table it can be seen that the results from the implemented method agree well with the results calculated from analytical solution within 95% confidence intervals.

In true analog calculation, it is started from any instantaneous source distribution, that is the initial condition *N(0)* and it is followed the evolution of neutron density in time. Figure 4.1 represents the linear increase in neutron density with time on logarithmic plot. The secondary y-axis represents the relative standard deviation with the evolution of neutron density in time. The lower right corner plot is a view of some part of the logarithmic plot represents the exponential increase in neutron density with time.

It is analyzed that there is a propagation in statistical uncertainty in neutron density. Table 4.3 shows the numerical results for the

propagation in standard deviation for neutron density tally and real standard deviation of the mean for 100 independent TDMC simulations. It is observed that the results are within 95% confidence intervals. Figure 4.2 represents the propagation in standard deviation in neutron density with time by using proposed uncertainty propagation model compared with the real standard deviation (RSD).

Table 4.2: Comparison of neutron densities for one-group infinite homogeneous problem

Time (s)	Neutron Density		Relative Std. Dev. (RSD) [%]
	Analytical Solution	TDMC Solution	
1.00×10^{-9}	1.40820×10^{4}	1.41570×10^{4}	0.84
2.00×10^{-9}	1.98304×10^{4}	1.99911×10^{4}	0.83
3.00×10^{-9}	2.79253×10^{4}	2.79176×10^{4}	0.83
4.00×10^{-9}	3.93245×10^{4}	3.93638×10^{4}	0.84
5.00×10^{-9}	5.53770×10^{4}	5.51920×10^{4}	0.82
6.00×10^{-9}	7.79821×10^{4}	7.81573×10^{4}	0.83
7.00×10^{-9}	1.09815×10^{5}	1.09866×10^{5}	0.83
8.00×10^{-9}	1.54642×10^{5}	1.54878×10^{5}	0.85
9.00×10^{-9}	2.17767×10^{5}	2.19756×10^{5}	0.84
1.00×10^{-8}	3.06661×10^{5}	3.05351×10^{5}	0.84
1.10×10^{-8}	4.31842×10^{5}	4.38545×10^{5}	0.86
1.20×10^{-8}	6.08121×10^{5}	6.23874×10^{5}	0.86
1.30×10^{-8}	8.56360×10^{5}	8.91953×10^{5}	0.84
1.40×10^{-8}	1.20593×10^{6}	1.26711×10^{6}	0.85
1.50×10^{-8}	1.69820×10^{6}	1.81159×10^{6}	0.84
1.60×10^{-8}	2.39141×10^{6}	2.55289×10^{6}	0.85
1.70×10^{-8}	3.36759×10^{6}	3.56664×10^{6}	0.85
1.80×10^{-8}	4.74226×10^{6}	5.04287×10^{6}	0.83
1.90×10^{-8}	6.67808×10^{6}	7.13263×10^{6}	0.84

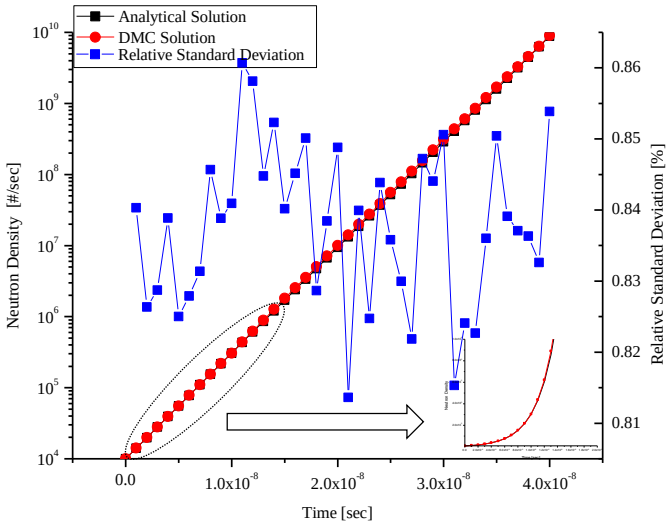

Figure 4.1: Exponential variation of neutron density tally with time

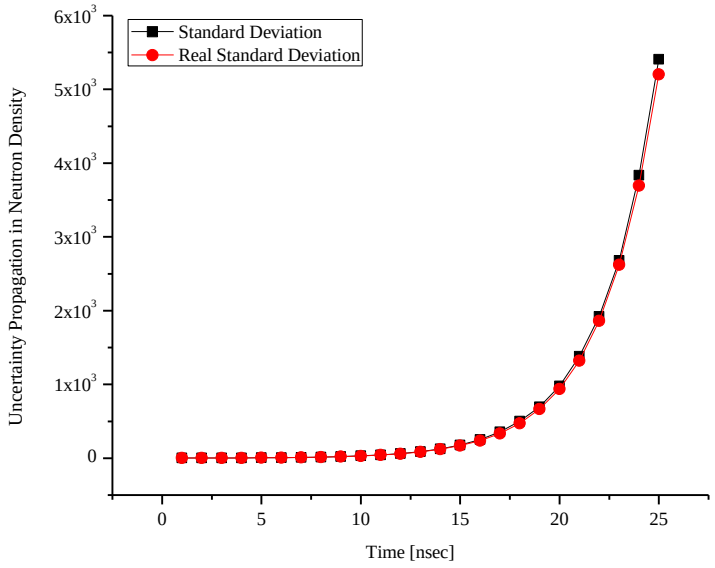

Figure 4.2: Standard deviation vs real standard deviation

Table 4.3: Comparison of Standard Deviation and Real Standard Deviation in Neutron Densities

Time (s)	Std. Dev. in Neutron Density	Real Standard Deviation [RSD]	Difference
1.0×10^{-9}	1.402×10^{0}	1.404×10^{0}	-0.002
2.0×10^{-9}	1.963×10^{0}	1.978×10^{0}	-0.015
3.0×10^{-9}	2.776×10^{0}	2.784×10^{0}	-0.008
4.0×10^{-9}	3.886×10^{0}	3.914×10^{0}	-0.028
5.0×10^{-9}	5.518×10^{0}	5.517×10^{0}	0.001
6.0×10^{-9}	7.820×10^{0}	7.776×10^{0}	0.044
7.0×10^{-9}	1.103×10^{1}	1.095×10^{1}	0.08
8.0×10^{-9}	1.574×10^{1}	1.544×10^{1}	0.3
9.0×10^{-9}	2.188×10^{1}	2.171×10^{1}	0.17
1.0×10^{-8}	3.154×10^{1}	3.058×10^{1}	0.96
1.1×10^{-8}	4.434×10^{1}	4.303×10^{1}	1.31
1.2×10^{-8}	6.279×10^{1}	6.057×10^{1}	2.22
1.3×10^{-8}	8.828×10^{1}	8.544×10^{1}	2.84
1.4×10^{-8}	1.269×10^{2}	1.204×10^{2}	6.5
1.5×10^{-8}	1.795×10^{2}	1.694×10^{2}	10.1
1.6×10^{-8}	2.513×10^{2}	2.381×10^{2}	13.2
1.7×10^{-8}	3.550×10^{2}	3.359×10^{2}	19.1
1.8×10^{-8}	5.006×10^{2}	4.729×10^{2}	27.7
1.9×10^{-8}	6.940×10^{2}	6.659×10^{2}	28.1

4.2.2 Infinite Homogeneous Two-Group Problem

Two-group infinite homogeneous problem with speeds, υ_1 and υ_2 is considered as a simplest non-trivial example. It is assumed that neutrons are transported in an infinite media with no up-scattering, that there is an emission of prompt neutrons only in group $g = 1$. If there is no external source then the time-dependent two group neutron transport equations for flux distribution can be interpreted as [22];

$$\begin{aligned} &\frac{1}{\upsilon_1}\frac{\partial \phi_1}{\partial t} + \Sigma_{t1}\phi_1 = \Sigma_{s11}\phi_1 + \Sigma_{s12}\phi_2 \\ &\frac{1}{\upsilon_2}\frac{\partial \phi_2}{\partial t} + \Sigma_{t2}\phi_2 = \Sigma_{s22}\phi_2 + \nu_1\Sigma_{f1}\phi_1 + \nu_2\Sigma_{f2}\phi_2 \end{aligned} \qquad (4.9)$$

The solution of above system of equations gives group flux. To calculate the group neutron density, group flux is divided by the corresponding group neutron speed. The reference physical parameters for a super-critical infinite homogeneous problem with $k_\infty = 1.10075$ are given in Table 4.4.

The results of the TDMC simulations for 10,000 neutron histories and 200 time steps with time step size 10.0 μs are interpreted in Table 4.5 and compared with the solution found by MATLAB. Figure 4.3 and Figure 4.4 represent the neutron density in first and second energy groups

respectively along with the variation in relative standard deviation.

Numerical results for standard deviation and real standard deviation computed for 100 independent simulations for the neutron density are shown in Table 4.6. It is observed that the results are within 95% confidence intervals. Figure 4.5 represents the propagation in standard deviation in neutron density with time by using proposed uncertainty propagation model compared with the real standard deviation (RSD) in both the energy groups.

Table 4.4: Two-group cross sections for infinite homogeneous problem

Cross Section	First Group (g=1)	Second Group (g=2)
ν_g	2.50	2.70
Σ_{fg}	0.06912	0.06192
Σ_{ag}	0.13862	0.16142
Σ_{sgg}	0.26304	0.078242
$\Sigma_{sg'g}$ $(g' \neq g)$	0.0	0.072
Σ_{tg}	0.40166	0.31166
χ_g	0.0	1.0
$1/\upsilon_g$ [sec/cm]	9.14505×10^{-7}	7.22980×10^{-7}

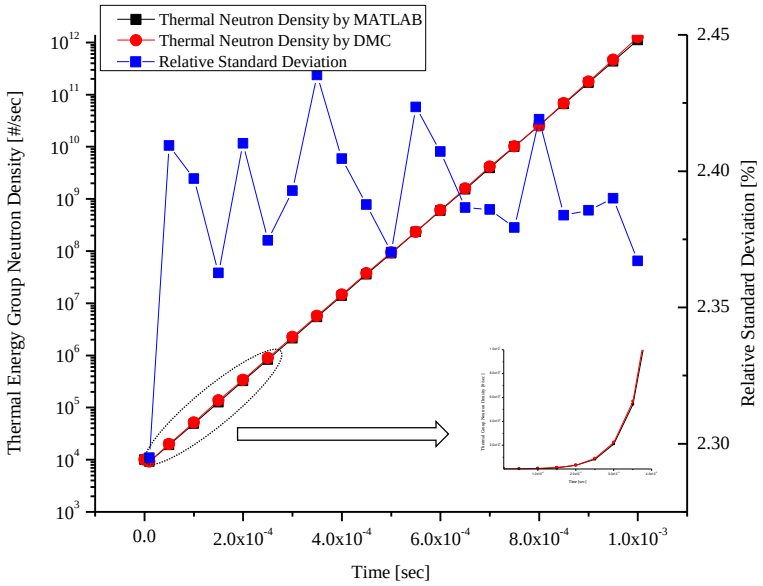

Figure 4.3: Neutron density in first energy group

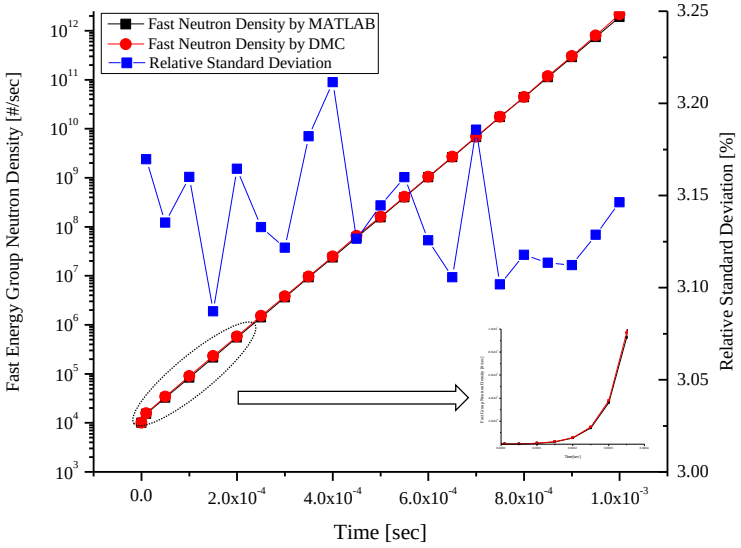

Figure 4.4: Neutron density in second energy group

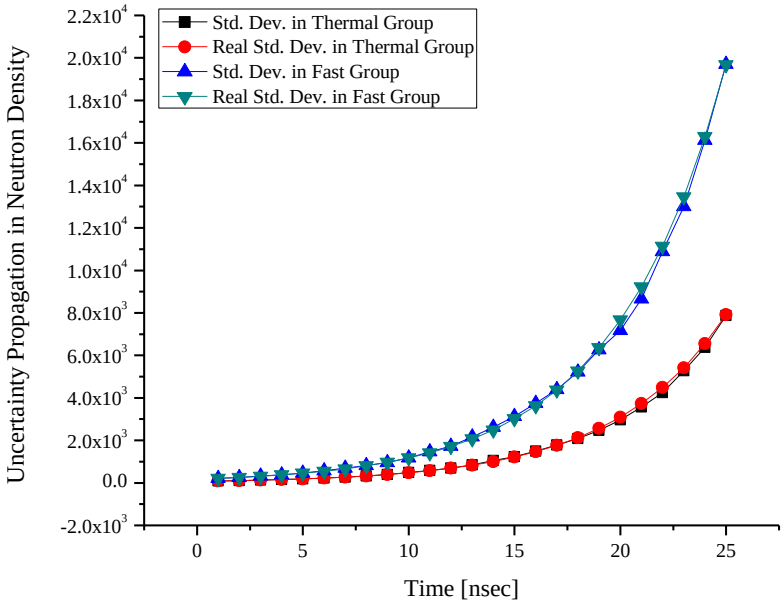

Figure 4.5: Standard deviation vs real standard deviation.

Table 4.5: Comparison of neutron densities for two-group infinite homogeneous problem

Time (s)	Neutron Density (MATLAB Solution)		Neutron Density (TDMC Solution)		Relative Std. Dev. (RSD) [%]	
	First Group	Second Group	First Group	Second Group	First Group	Second Group
1.0×10^{-5}	9.22414×10^{3}	1.52169×10^{4}	9.26600×10^{3}	1.56180×10^{4}	2.29	3.17
5.0×10^{-5}	1.91845×10^{4}	3.27403×10^{4}	1.99110×10^{4}	3.42428×10^{4}	2.41	3.14
1.0×10^{-4}	4.91904×10^{4}	8.38535×10^{4}	5.18764×10^{4}	8.95993×10^{4}	2.40	3.16
1.5×10^{-4}	1.26036×10^{5}	2.14864×10^{5}	1.36989×10^{5}	2.30874×10^{5}	2.36	3.09
2.0×10^{-4}	3.22808×10^{5}	5.50701×10^{5}	3.41171×10^{5}	5.77859×10^{5}	2.41	3.16
2.5×10^{-4}	8.26774×10^{5}	1.41147×10^{6}	8.95560×10^{5}	1.51842×10^{6}	2.37	3.13
3.0×10^{-4}	2.11904×10^{6}	3.61598×10^{6}	2.26043×10^{6}	3.80371×10^{6}	2.39	3.12
3.5×10^{-4}	5.43277×10^{6}	9.26183×10^{6}	5.70027×10^{6}	9.67843×10^{6}	2.44	3.18
4.0×10^{-4}	1.39216×10^{7}	2.37304×10^{7}	1.47221×10^{7}	2.48614×10^{7}	2.40	3.21
4.5×10^{-4}	3.56597×10^{7}	6.08179×10^{7}	3.77051×10^{7}	6.54494×10^{7}	2.39	3.13
5.0×10^{-4}	9.13504×10^{7}	1.55858×10^{8}	9.44370×10^{7}	1.61481×10^{8}	2.37	3.14
5.5×10^{-4}	2.34109×10^{8}	3.99311×10^{8}	2.34241×10^{8}	4.06923×10^{8}	2.42	3.16
6.0×10^{-4}	5.99865×10^{8}	1.02316×10^{9}	6.10370×10^{8}	1.05023×10^{9}	2.41	3.13
6.5×10^{-4}	1.53744×10^{9}	2.62121×10^{9}	1.57753×10^{9}	2.69890×10^{9}	2.39	3.11
7.0×10^{-4}	3.93582×10^{9}	6.72033×10^{9}	4.17350×10^{9}	6.88929×10^{9}	2.39	3.19
7.5×10^{-4}	1.00854×10^{10}	1.72189×10^{10}	1.02135×10^{10}	1.74681×10^{10}	2.38	3.10
8.0×10^{-4}	2.58551×10^{10}	4.41058×10^{10}	2.53491×10^{10}	4.45106×10^{10}	2.42	3.12
8.5×10^{-4}	6.63131×10^{10}	1.12942×10^{11}	6.85577×10^{10}	1.17610×10^{11}	2.38	3.11
9.0×10^{-4}	1.69819×10^{11}	2.89499×10^{11}	1.76957×10^{11}	3.04030×10^{11}	2.39	3.11

Table 4.6: Comparison of standard deviation and real standard deviation in neutron densities

Time (s)	Standard Deviation		Real Standard Deviation		Difference	
	First Group	Second Group	First Group	Second Group	First Group	Second Group
$1.0x10^{-5}$	$8.620x10^{1}$	$2.131x10^{2}$	$8.609x10^{1}$	$2.145x10^{2}$	0.11	-1.43
$5.0x10^{-5}$	$1.064x10^{2}$	$2.577x10^{2}$	$1.044x10^{2}$	$2.585x10^{2}$	2.08	-0.87
$1.0x10^{-4}$	$1.281x10^{2}$	$3.177x10^{2}$	$1.262x10^{2}$	$3.133x10^{2}$	1.88	4.37
$1.5x10^{-4}$	$1.552x10^{2}$	$3.811x10^{2}$	$1.527x10^{2}$	$3.783x10^{2}$	2.50	2.88
$2.0x10^{-4}$	$1.824x10^{2}$	$4.646x10^{2}$	$1.835x10^{2}$	$4.552x10^{2}$	-1.14	9.38
$2.5x10^{-4}$	$2.270x10^{2}$	$5.695x10^{2}$	$2.215x10^{2}$	$5.482x10^{2}$	5.50	21.32
$3.0x10^{-4}$	$2.753x10^{2}$	$6.950x10^{2}$	$2.674x10^{2}$	$6.612x10^{2}$	7.87	33.87
$3.5x10^{-4}$	$3.247x10^{2}$	$8.209x10^{2}$	$3.223x10^{2}$	$8.013x10^{2}$	2.38	19.67
$4.0x10^{-4}$	$3.944x10^{2}$	$9.570x10^{2}$	$3.897x10^{2}$	$9.672x10^{2}$	4.73	-10.20
$4.5x10^{-4}$	$4.903x10^{2}$	$1.182x10^{3}$	$4.722x10^{2}$	$1.171x10^{3}$	18.06	11.56
$5.0x10^{-4}$	$5.888x10^{2}$	$1.462x10^{3}$	$5.690x10^{2}$	$1.416x10^{3}$	19.79	45.85
$5.5x10^{-4}$	$7.001x10^{2}$	$1.726x10^{3}$	$6.890x10^{2}$	$1.708x10^{3}$	11.08	18.43
$6.0x10^{-4}$	$8.406x10^{2}$	$2.172x10^{3}$	$8.319x10^{2}$	$2.067x10^{3}$	8.65	104.56
$6.5x10^{-4}$	$1.057x10^{3}$	$2.626x10^{3}$	$1.005x10^{3}$	$2.490x10^{3}$	52.70	135.49
$7.0x10^{-4}$	$1.230x10^{3}$	$3.136x10^{3}$	$1.212x10^{3}$	$3.022x10^{3}$	17.51	113.70
$7.5x10^{-4}$	$1.492x10^{3}$	$3.747x10^{3}$	$1.465x10^{3}$	$3.627x10^{3}$	26.12	120.39
$8.0x10^{-4}$	$1.788x10^{3}$	$4.392x10^{3}$	$1.764x10^{3}$	$4.372x10^{3}$	23.90	20.30
$8.5x10^{-4}$	$2.087x10^{3}$	$5.227x10^{3}$	$2.120x10^{3}$	$5.266x10^{3}$	-32.19	-39.08
$9.0x10^{-4}$	$2.476x10^{3}$	$6.260x10^{3}$	$2.561x10^{3}$	$6.358x10^{3}$	-84.46	-98.31

CHAPTER. 5 Conclusions and Future Work

5.1 General Conclusions

In this thesis, the time-dependent Monte Carlo (TDMC) algorithm with coming technique to control the neutron population for off-critical systems is implemented. Instead of considering the cycles, the simulation is divided in time intervals. At the end of each time interval, neutron population control is applied on the banked neutrons. Randomly selected neutrons are discarded, until the size of neutron population matches the initial neutron histories at the beginning of time simulation.

The prompt neutron decay constant α is estimated from TDMC algorithm for subcritical systems. The effectiveness of the results is examined for two-group infinite homogeneous problems with varying the *k*-value. From the comparisons with the analytical solutions, it is observed that the results are quite comparable with each other for each *k*-value. The applicability of the TDMC module is also evaluated for an experimental benchmark of the thorium-loaded accelerator-driven system. From the comparison of α's calculated by the TDMC simulations with those from measurements, MC α-iteration algorithm and MC PNS

simulations, it is seen that the α results are quite comparable with each other for the cases where the experiments provide reliable estimates.

The implementation of the dynamic method in standard static McCARD has shown its general applicability. The results of the TDMC module demonstrate not only the general applicability of the new methods, but also the practical feasibility of a transient analysis in realistic complex geometry. The TDMC steady state initial condition modeling presented in this thesis is a novel and unique method. We develop a new MC steady-state simulation suited to generate the prompt neutron sources and the delayed neutron precursors for the MC transient simulations. The proposed TDMC steady-state simulation method accompanied with the Sjenitzer and Hoogenboom's delayed neutron handling algorithm and the analog MC branching process simulation method with the combing technique is applied for the time-dependent MC analysis of the 2D C5G7-TD kinetics problems. From the numerical results, it is demonstrated that the McCARD TDMC results are quite comparable with those from a deterministic transport analysis code, nTRACER.

The main advantage of the Monte Carlo method is that no

system-specific approximations are used and therefore it is generally applicable. Due to the high computational cost, the main application will be to act as a validation tool for the computationally less expensive deterministic methods.

For the transient analysis with temperature feedback, a dynamic MC simulation capability in McCARD is coupled with the computational fluid dynamics code CUPID using the socket communication. The McCARD/CUPID transient analysis is performed for a hypothetical problem based on a triangular unit cell model in the IAEA CRP HTGR UAM benchmark to analyze a transient of about 3 seconds.

5.2 Validation

The calculations shown in this thesis demonstrate the feasibility of performing a transient analysis for only C5G7-TD benchmark and the coupled Monte Carlo neutronics/thermal-hydraulics calculation with a small hypothetical triangular unit cell model. It is needed to validate these calculations with more benchmarks for the transient analysis of realistic geometries. However, it has not been possible yet to validate these calculations completely for the coupled code, even though it could

be possible to get the meaningful results. A future challenge lies in the validation of the dynamic Monte Carlo method and its implementation in the standard McCARD. The method should be benchmarked against real-life, well-documented experiments. Furthermore, it is necessary to further investigate the effects of the variance on the coupling mechanism.

5.3 Further Developments

Since, it is a new era in the field of time-dependent Monte Carlo method for the transient analysis of nuclear reactors. It is needed to enhance the capability of the TDMC scheme as well as the coupled scheme to check their validation for real and well documented benchmarks. After this demonstration, the next step is to further improve the simulation scheme and Monte Carlo techniques. The efficiency of the calculation can be improved by implementing the latest methodologies proposed by the other active research groups working in the field of dynamic Monte Carlo. Another novel improvement can be found in enabling the internal coupling of neutronics module with the thermal hydraulic module already implemented in McCARD in addition to the generation of temperature-dependent cross sections produced by a built-in on-the-fly Doppler broadening (OTF DB) module. Successful

implementation of one of these multiple novel techniques can also make the dynamic simulation more accurate.

All in all, it has been shown that it is feasible to perform time-dependent Monte Carlo method for the analyses on nuclear reactor systems. The main task is now to make this method capable of analyzing the transient behavior of all kind of newly proposed reactor geometries for further refinement.

References

1. B. L. Sjenitzer and J. E. Hoogenboom, “Dynamic Monte Carlo Method for Nuclear Reactor Kinetics Calculations,” Nucl. Sci. Eng., 175, 94 (2013).

2. B. L. Sjenitzer, J. E. Hoogenboom, J. J. Escalante, V. S. Espinoza, “Coupling of Dynamic Monte Carlo with Thermal-Hydraulic Feedback,” Ann. Nucl. Energy, 76, 27 (2015).

3. Y. G. Jo, B. Cho, N. Z. Cho, “Nuclear Reactor Transient Analysis by Continuous-Energy Monte Carlo Calculation Based on Predictor-Corrector Quasi-Static Method,” Nucl. Sci. Eng., 183, 229 (2016).

4. E. L. Kaplan, “Monte Carlo Methods for Equilibrium Solutions in Neutron Multiplication,” UCRL-5275-T, Lawrence Livermore National Laboratory (1958).

5. L. M. Petrie and N. F. Cross, "KENO-V.a: An Improved Monte Carlo Criticality Program with Supergrouping," NUREG/CR-0200, Sec. Fll, ORNL/NUREG/CSD-2, Vol. 2, Oak Ridge National Laboratory

(1985).

6. ‘‘MCNP—A General Monte Carlo N-Particle Transport Code, Version 4A,’’ LA-12625, J. F. Briesmeister, Ed., Los Alamos National Laboratory (1993).

7. J. T. Mihalczo and T. E. Valentine, “Calculational Verification and Process Control Applications Utilizing the High Sensitivity of Noise Measurement Parameters to Fissile System Configuration,” Nucl. Sci. Eng., 121, 286 (1995).

8. T. E. Valentine and J. T. Mihalczo, “MCNP-DSP: A Neutron and Gamma Ray Monte Carlo Calculation of Source-Driven Noise-Measured Parameters,” Ann. Nucl. Energy, 23(16), 1271 (1996).

9. U. Wiącek, E. Krynicka, “Decay of the pulsed thermal neutron flux in two-zone hydrogenous systems – Monte Carlo simulations using MCNP standard data libraries,” Nuclear Instruments and Methods in Physics Research Section B: Beam Interactions with Materials and Atoms, 243(1), 92 (2006).

10. D. E. Cullen, “TART 2002: A Coupled Neutron-Photon, 3-D, Combinatorial Geometry, Time Dependent Monte Carlo Transport Code”, UCRL-ID-126455, Rev. 4, Lawrence Livermore National Laboratory (2002).

11. T. E. Booth, “A Weight (Charge) Conserving Importance-Weighted Comb for Monte Carlo,” LA-UR--96-0051, Los Alamos National Laboratory (1996).

12. D. E. Cullen, C. J. Clouse, R. Procassini, R. C. Little, “Static and Dynamic Criticality: Are They Different?,” UCRL-TR-201506, Lawrence Livermore National Laboratory (2003).

13. D. Brockway, P. Soran, P. Whalen, “Monte Carlo α calculation,” LA-UR-85-1224, Los Alamos National Laboratory (1985).

14. C. H. Pyeon, “Experimental Benchmarks on Thorium-Loaded Accelerator-Driven System at Kyoto University Critical Assembly,” KURR-TR(CD)-48, Research Reactor Institute, Kyoto University (2015).

15. N. Shaukat and H. J. Shim, “Alpha Eigenvalue Estimation from Dynamic Monte Carlo Calculation for Subcritical Systems,” Transactions of the Korean Nuclear Society Spring Meeting, Jeju, Korea, May 11-13 (2016).

16. H. J. Shim, S. H. Jang, and S. M. Kang, “Monte Carlo Alpha Iteration Algorithm for a Subcritical System Analysis,” Science and Technology of Nuclear Installations, vol. 2015, Article ID 859242, 7 pages (2015). doi:10.1155/2015/859242

17. H. J. Shim, B. S. Han, J. S. Jung, H. J. Park, C. H. Kim, “McCARD: Monte Carlo Code for Advanced Reactor Design and Analysis,” Nucl. Eng. Technol., 44(2), 161 (2012).

18. M. Aufiero, C. Fiorina, A. Laureau, P. Rubiolo, and V. Valtavirta, “Serpent–OpenFoam Coupling in Transient Mode: Simulation of a Godiva Prompt Critical Burst,” Proceedings of ANS MC2015–Joint International Conference on Mathematics and Computation (M&C), Supercomputing in Nuclear Applications (SNA) and the Monte Carlo (MC) Method, Nashville, TN (2015).

19. J. Lieberoth, “A Monte Carlo Technique to Solve the Static Eigenvalue Problem of the Boltzmann Transport Equation,” Nukleonik, 11, 213 (1968).

20. H. Y. Yoon, et al., “CUPID code manual vol.1: Mathmatical Models and Solution Methods,” Korea Atomic Energy Research Institute, KAERI/TR-4403/2011 (2011).

21. T. YAMAMOTO, Y. MIYOSHI, An Algorithm of α- and γ-Mode Eigenvalue Calculations by Monte Carlo Method, Japan Atomic Energy Research Institute, Tokai-mura, Naka-gun, Ibaraki 319-1195, Japan.

22. A. Zoia, E. Brun, and F. Malvagi, “A Monte Carlo method for prompt and delayed alpha eigenvalue calculations,” in Proceedings of the International Conference on the Role of Reactor Physics Toward a Sustainable Future (PHYSOR ’14), CD-ROM, Kyoto, Japan, September-October 2014.

23. V. F. Boyarinov, P. A. Fomichenko, J. Hou, K. Ivanov, A. Aures, W. Zwermann, K. Velkov, “Deterministic Time-Dependent Neutron

Transport Benchmark without Spatial Homogenization (C5G7-TD), Version 1.6," NEA/NSC/DOC(2016), OECD Nuclear Energy Agency (2016).

24. Y. S. Jung, C. B. Shim, C. H. Lim, H. G. Joo, "Practical Numerical Reactor Employing Direct Whole Core Neutron Transport and Subchannel Thermal/Hydraulic Solvers," Ann. Nucl. Energy, 62, 357 (2013).

25. "IAEA CRP on HTGR Reactor Physics, Thermal-hydraulics and Depletion Uncertainty Analysis," Draft revision 4, International Atomic Energy Agency (2014).

26. V. Valtavirta, "Uncertainty Underprediction in Coupled Time-Dependent Monte Carlo Simulations with SERPENT 2", Joint International Conference on Mathematics and Computation (M&C), Nashville, Tennessee, April 19-23, 2015.

27. V. Mahadevan, J. Ragusa and V. Mousseau, "A Verification Exercise in Multiphysics Simulations for Coupled Reactor Physics Calculations", Progress in Nuclear Energy, 2011.

28. J. Watson and K. Ivanov, “Demonstration of Implicit Coupling of TRACE/PARCS using Simplified One-Dimensional Problems”, Nuclear Technology, 180, 174, 2012.

29. K. Ivanov and M. Avramova, “Challenges in coupled thermal-hydraulics and neutronics simulations for LWR safety analysis”, Ann. Nucl. Energy, 34, 501, 2007.

30. F. Brown et al, “Advanced Monte Carlo for Reactor Physics Core analysis”, In Workshop at PHYSOR-2008, Interlaken, Switzerland, 14-9, 2008.

31. F. P. Espel et al., “New developments of the MCNP/CTF/NEM/NJOY Code System-Monte Carlo Based Coupled Code for High Accuracy Modeling”, Ann. Nucl. Energy, 51,18, 2013.

32. J. E. Hoogenboom et al., “A flexible coupling scheme for Monte Carlo and thermal-hydraulics codes”, In Proceedings of M&C conference. Riode Janeiro, 2011.

33. G.Yesilyurt, W. Martin and F. Brown, “On-the-fly Doppler Broadening or Monte Carlo Codes. Nuclear Science and Engineering,

171, 239, 2012.

34. M. Armishaw et al. “The ANSWERS code MONK-a new Approach to Scoring, Tracking, Modelling and Visualisation”, In Proceedings of 9th International Conference on Nuclear Criticality Safety (ICNC2011), Edinburgh, UK, 2011.

35. T. Viitanen and J. Leppänen, “Explicit Treatment of Thermal Motion in Continuous-Energy Monte Carlo Tracking Routines”, Nuclear Science and Engineering, 171, 165, 2012.

36. A. Zoia et al., “Doppler Broadening of Neutron Elastic Scattering Kernel in Tripoli-4”, Annals of Nuclear Energy, 54, 218, 2013.

37. B. L. Sjenitzer, “Temperature Dependent Monte Carlo Simulation: Thermalization”, Technical Report, Delft University of Technology/Commissariat à l’Énergieatomique, 2009.

초록

원자로 과도상태 해석을 위한 효과적인 시간종속 몬테카를로 중성자 모의법 개발

쇼컷 나딤

원자력 공학박사

에너지시스템 공학부

서울대학교 대학원

시간에 따른 중성자의 점근적 거동은 원자로 시동 분석, 반응도 측정 및 가속기 구동 시스템의 동역학과 관련된 주제들을 연구함으로써 평가할 수 있으며 이것은 시간 종속 볼츠만 중성자 수송 방정식을 푸는 것과 같다. 통상적인 코밍(combing) 방법을 통해 시간에 따른 중성자의 수를 제어하는 시간 종속 몬테칼로(TDMC)

알고리즘을 McCARD에 구현하였다.

미임계 시스템의 TDMC 계산을 통해 알파 고유치를 추정하였다. 제어봉 모델 및 다양한 미임계도를 가지는 2군 무한균질문제에 대해 계산 결과와 해석해를 비교하여 유효성을 평가하였다. 또한 교토 대학교 임계 집합체(KUCA)의 토륨 장전 가속기 구동 시스템 실험 검증문제에 대해 알파 값을 계산하였고 이를 측정값 및 몬테칼로 알파 반복법, 몬테칼로 펄스 중성자 선원(PNS) 시뮬레이션 결과와 비교하여 그 적용성을 평가하였다.

컴퓨터 기술의 지속적인 발전으로 몬테칼로 중성자 수송 계산은 활용 분야가 확장되어 원자로 과도해석에까지 적용되고 있다. 원자로 과도해석을 위한 시간 종속 몬테칼로 (TDMC) 중성자 추적은 지발 중성자 생성, 중성자 수 제어 및 초기 조건의 모델링을 위한 효율적인 알고리즘이 필요하다. 본 연구에서는 과도해석의 초기 조

건인 즉발 중성자 선원과 지발 중성자 선행핵 분포를 쉽게 샘플링 할 수 있는 TDMC 기반의 새로운 정상상태 몬테칼로 시뮬레이션 방법을 제안하였다. 과도해석을 위한 TDMC 기반 정상상태 시뮬레이션 방법은 McCARD에 구현되었으며 시간 종속 중성자 수송 검증문제인 C5G7-TD 중 온도 궤환효과를 고려하지 않는 2차원 노심 동특성 문제에 적용되었다. McCARD TDMC 계산 결과는 결정론적 수송 해석 코드인 nTRACER의 결과와 잘 일치했다. 원자로 과도해석은 또한 열수력 궤환효과를 고려한 중성자 수송 계산을 필요로 한다. 본 연구에서는 열수력 궤환효과를 고려한 원자로 과도 해석을 위해 TCP/IP 소켓 통신을 이용하여 McCARD TDMC 모듈과 전산 유체 역학 코드인 CUPID를 결합하였다. McCARD/CUPID 과도 계산에 사용된 온도에 따른 핵반응 단면적 데이터는 McCARD에 내장되어 있는 계산중 도플러 단면적 확장 (OTF DB) 모듈을 통해 생산하

였다. McCARD/CUPID 과도해석 결과는 IAEA 국제 공동 연구 프로젝트 (CRP)의 고온가스로 (HTGR) 불확도 분석 검증문제 중 가상의 삼각형 단위셀 문제에 대해 그 유효성을 평가하였다.

한 시간 구간에서의 통계적 불확실도는 이전 시간 구간에서의 계산 결과를 오차 전파하여 추정하였다. 전형적인 오차전파 방법을 통해 계산 결과의 불확실도가 시스템을 통해 어떻게 전파되는지 연구하였다.

주요어:

시간 종속 몬테칼로

알파 고유치 추정

원자로 과도해석

C5G7-TD 검증문제

학번 **: 2013-30779**